



HAL
open science

Vertical Mixing Effects on Phytoplankton Dynamics and Organic Carbon Export in the Western Mediterranean Sea

Fayçal Kessouri, Caroline Ulses, Claude Estournel, Patrick Marsaleix, Fabrizio d'Ortenzio, Tatiana Severin, Vincent Taillandier, Pascal Conan

► **To cite this version:**

Fayçal Kessouri, Caroline Ulses, Claude Estournel, Patrick Marsaleix, Fabrizio d'Ortenzio, et al.. Vertical Mixing Effects on Phytoplankton Dynamics and Organic Carbon Export in the Western Mediterranean Sea. *Journal of Geophysical Research. Oceans*, 2018, 123 (3), pp.1647-1669. 10.1002/2016JC012669 . hal-02322803

HAL Id: hal-02322803

<https://hal.science/hal-02322803>

Submitted on 15 Feb 2021

HAL is a multi-disciplinary open access archive for the deposit and dissemination of scientific research documents, whether they are published or not. The documents may come from teaching and research institutions in France or abroad, or from public or private research centers.

L'archive ouverte pluridisciplinaire **HAL**, est destinée au dépôt et à la diffusion de documents scientifiques de niveau recherche, publiés ou non, émanant des établissements d'enseignement et de recherche français ou étrangers, des laboratoires publics ou privés.

21 **Abstract**

22 A 3D high-resolution coupled hydrodynamic-biogeochemical model of the western
23 Mediterranean was used to study phytoplankton dynamics and organic carbon export in three
24 regions with contrasting vertical regimes, ranging from deep convection to a shallow mixed
25 layer. One month after the initial increase in surface chlorophyll (caused by the erosion of the
26 deep chlorophyll maximum), the autumnal bloom was triggered in all three regions by the
27 upward flux of nutrients resulting from mixed layer deepening. In contrast, at the end of winter,
28 the end of turbulent mixing favored the onset of the spring bloom in the deep convection region.
29 Low grazing pressure, due to convection-induced dilution in winter that reduced prey–predator
30 interactions, allowed rapid phytoplankton growth during the bloom. Primary production in the
31 Algerian subbasin was characterized by a long period of sustained phytoplankton development
32 and permanent stratified conditions, unlike the deep convection region where primary production
33 was inhibited during two months in winter. Despite seasonal variations, annual primary
34 production in all three regions is similar. In the deep convection region, total organic carbon
35 export below the photic layer (150m) and transfer to deep waters (800m) was 5 and 8 times,
36 respectively, higher than in the Algerian subbasin. Up to 45% of the organic matter deeply
37 exported has been laterally transported out of the deep convection region. The Mediterranean Sea
38 is considered as a hotspot of climate change and understanding changes in its ecosystem in future
39 decades could offer an insight into the evolution of the functioning of the global ocean.

40 **Index Terms and Keywords**

41 Biogeochemical cycles, processes, and modeling, Upper ocean and mixed layer processes,
42 Phytoplankton, Marginal and semi-enclosed seas.

43 Physical-biogeochemical 3D ocean modeling, western Mediterranean Sea, deep convection,

44 phytoplankton bloom, primary production, carbon deep export

45 **1. Introduction**

46 The mixed layer depth (MLD) is considered to be a major factor in controlling phytoplankton
47 development [Sverdrup, 1953]. At large scales, gyre circulation leads to surface waters being
48 nutrient-rich over subpolar gyres, and nutrient-poor over subtropical gyres [Williams and
49 Follows, 2003]. The subpolar winter regime is characterized by a deepening of the mixed layer
50 by several hundreds of meters and a large supply of inorganic nutrients in surface waters, while
51 phytoplankton growth is limited by a lack of light when cells are transferred below the photic
52 zone. In spring, an intense phytoplankton development occurs when the mixed layer shoals or,
53 more generally, when turbulent mixing becomes weak [Taylor and Ferrari, 2011]. This can be
54 compared to the subtropical regime, where the deepening of the mixed layer to ~100 m, and
55 phytoplankton growth co-occur. Under this regime, phytoplankton development is triggered by
56 the mixing-induced supply of nutrients.

57 Export of organic carbon towards the deep ocean may play a determining role in sustaining
58 mesopelagic ecosystems [Giering et al., 2017] and in sequestration of atmospheric carbon. This
59 export exhibits large-scale variability in response to the variability of the MLD and plankton
60 dynamics. Various authors have made satellite-based estimates of the global export, and pointed
61 out high export under the photic zone in subpolar oceans, and low export in subtropical gyres
62 [Henson et al. 2012; Laws et al, 2011; Westberry et al., 2012; Siegel et al., 2014]. These
63 satellite-base estimates attempt to account for export from the euphotic zone and their algorithms
64 likely do not account for export via the mixed layer pump. Gardner et al. [1995] suggested that
65 the alternation between periods of stratification, favoring phytoplankton growth, and periods of
66 mixed layer deepening enhances the efficiency of vertical export through the “mixed layer
67 pump” process. This consists in increasing, through mixing, the slow sinking rate of
68 phytoplankton and particles. Dall’Olmo et al. [2016] estimated that, in high latitudes, the ratio of

69 mixed layer pump to biological pump (fast sinking particles) is 23% on average, and can reach
70 over 100%.

71 The western Mediterranean Sea (Fig. 1) is characterized by the presence of subsurface water
72 masses with high MLD gradients over several hundred kilometers in the south–north direction.
73 Winter MLD values reach several hundred meters in the northwestern convection zone (Gulf of
74 Lions), and only 60–80 m in the Algerian sub-basin [*Houpert et al.*, 2015]. Furthermore,
75 D’Ortenzio and Ribera d’Alcala [2009] concluded that the western Mediterranean exhibits a
76 bloom-like regime that is similar to the subpolar regime in its chlorophyll concentration and
77 mixed layer seasonal evolution in the northwestern region, and a non-blooming behavior that is
78 similar to the subtropical regime in the south.

79 Observational studies conducted in the western Mediterranean have shown that particulate
80 organic carbon (POC) export fluxes below the euphotic layer and at mid-depth (1000 m) are
81 maximum during (February/ March) and/ or following winter mixing events (April, May, June)
82 (3 to 4 times higher than the rest of the year) [*Miquel et al.*, 2011; *Stabholz et al.*, 2013; *Gogou et*
83 *al.*, 2014]. The authors of these studies argued that the spring peak is caused by fertilization
84 induced by winter mixing, favoring a diatom-dominated ecosystem in the northwestern region.
85 Moreover, Avril [2002] observed the transfer of dissolved organic carbon (DOC) at the surface
86 to deep waters during intense vertical mixing in the northwestern region (DYFAMED station,
87 Fig. 1) and estimated that the winter mixing flux ($10 \text{ gC m}^{-2} \text{ year}^{-1}$) constituted 91% of the
88 annual flux at 100 m. Based on modeling studies, Ulses et al. [2016] found that the annual
89 amount of exported organic carbon at 100 m depth is primarily related to the intensity of the
90 deep convection process. They found that in years with strong convection, organic carbon export
91 was twice that of years with shallow convection. Export efficiency showed the same interannual
92 pattern, while the transfer to deep waters ($>1000 \text{ m}$) and the deposition on the seabed showed no

93 clear trend. Bernardello et al. [2012] also used a modeling approach, and stressed the importance
94 of the mixed layer pump in driving the interannual variability of POC export in the northwestern
95 Mediterranean region. However, estimates of primary production and export flux remain
96 uncertain in the western Mediterranean [Gogou et al., 2014] and, in general, for the global ocean
97 [Henson et al., 2012 ; Siegel et al., 2014; 2016]. Uncertainties in observational methods are
98 mainly associated with the scarcity of measurements, which cannot reflect interannual and
99 spatial variability. Other uncertainties arise from the lack of an overview of the system; for
100 example, limited information is available on degradation and recycling processes (such as
101 nitrification), and the contribution of DOC to total export. Estimates from modeling approaches,
102 which simplify the system and are poorly constrained by sparse observations, are also associated
103 with large uncertainties.

104 Modifications of water masses in the Mediterranean Sea have been observed since the 1990s and
105 are now impacting the whole basin [The MerMex Group, 2011]. Some have been partly
106 attributed to climatic variations. For example, the Eastern Mediterranean Transient has been
107 found to correspond to a switch in the region of deep water formation in the eastern
108 Mediterranean, from the Adriatic to the Aegean [Roether et al., 1996], which produced a rise in
109 the nutricline depth by 200–300 m [Klein et al., 1999]. In the western Mediterranean, an
110 acceleration of the increasing trend in salt and heat content in deep waters was reported
111 following an intense dense water formation event in 2004/ 2005 [Schroeder et al., 2010;
112 Borghini et al., 2014]. It is, however, increasingly clear that climate change is already impacting
113 water masses [Schroeder et al., 2016] and the ecosystem [Ben Rais Lasram et al., 2010]. The
114 Mediterranean Sea, which is characterized by a small spatial extent and mild meteorological
115 conditions that facilitate the deployment of instruments at sea, is an excellent laboratory to
116 monitor these impacts and to prepare models to predict future changes by calibrating them based
117 on the present transition period.

118 The impacts of climate change may include the frequency and/ or the intensity of convection,
119 which could be modified as a result of increasing stratification in the upper layers [*Somot et al.*,
120 2006]. The weakening of convection processes could lead to a reduction in the occurrence and
121 extent of phytoplankton blooms in the northwestern region. The consequences of climate change
122 on the structure of the planktonic ecosystem and carbon sequestration require further
123 examination. It is therefore a priority to better understand the functioning of the planktonic
124 ecosystem, within both convection and stratified regions of the western Mediterranean, and
125 assess how the ecosystem may evolve under weakened convection or in its absence.

126 In this context, and in the framework of the MerMex project, four cruises were carried out
127 between July 2012 and June 2013 [*Estournel et al.*, 2016a; *Waldman et al.*, 2016]. The data that
128 was collected made it possible to describe the spatial distribution of phytoplankton in the deep
129 convection northwestern Mediterranean during stratified, deep convection and phytoplankton
130 bloom periods [*Mayot et al.*, 2017a; *Severin et al.*, 2017]. This unprecedented *in situ* observation
131 offered a great opportunity to calibrate and validate a 3D coupled physical-biogeochemical
132 model [*Estournel et al.*, 2016b; *Kessouri et al.*, 2017]. In the present study, we used this coupled
133 model to investigate phytoplankton dynamics and the capacity of the western Mediterranean to
134 export organic carbon below the photic layer and to transfer it to deep waters. We focused on the
135 comparison of regions along a trophic and vertical mixing gradient encompassing the northern
136 and southern regions. These regions are characterized by a similar distribution of nutrients,
137 making it easier to discriminate the role of convection on primary production and export
138 variability from other possible influences.

139 The article starts with a presentation of the methods and an evaluation of the model's results. The
140 seasonal cycle of atmospheric forcing, MLD and chlorophyll vertical profile are presented in
141 Sections 4.1 and 4.2. The seasonal cycle of primary production and carbon export is described in

142 Sections 4.3 and 4.4, respectively. Finally, the conditions favoring bloom onset, export of
143 organic carbon under the photic zone, and its transfer to deep waters are discussed in Section 5.

144 **2. Methods**

145 **2.1 The numerical tool**

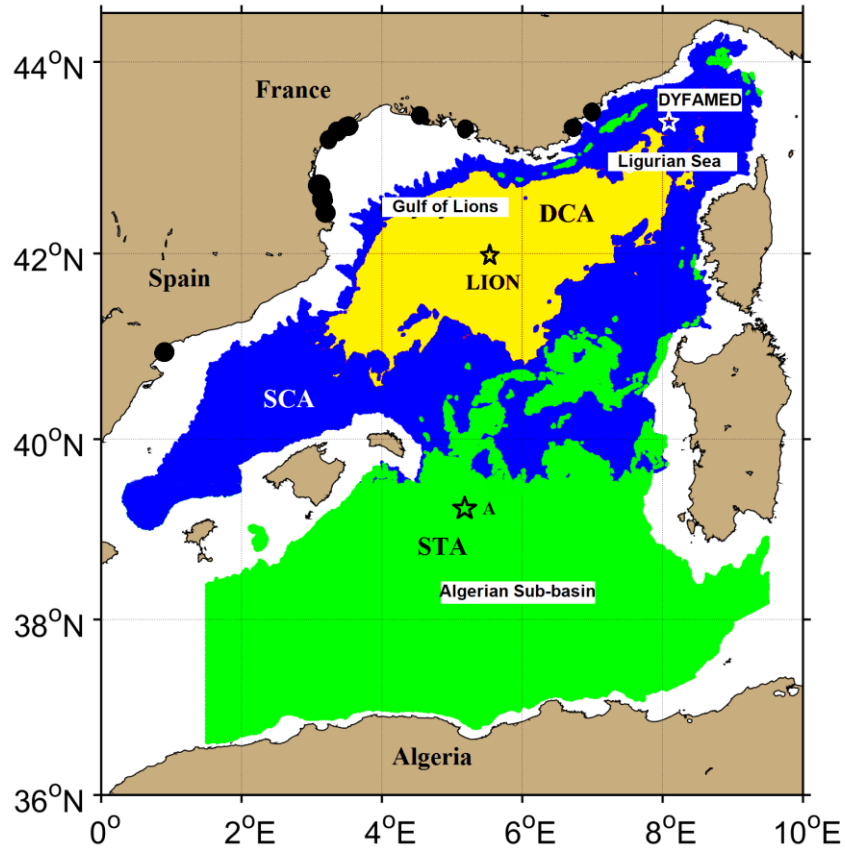
146 A biogeochemical model was forced offline using the daily outputs of a 3D hydrodynamic
147 model. The models and their initial and boundary conditions are described in the following
148 sections.

149 **2.1.1 The hydrodynamic model**

150 The SYMPHONIE model used in this study is a 3D primitive equation, with a free surface and
151 generalized sigma vertical coordinate, described in Marsaleix et al. [2008, 2009, 2011 and 2012].
152 This model was previously used in the Mediterranean to simulate open sea convection [*Estournel*
153 *et al.*, 2016b], and ocean circulation on the slope [*Rubio et al.*, 2009] and on the continental shelf
154 [*Petrenko et al.*, 2008]. The numerical domain (Figure 1) covered most of the western
155 Mediterranean basin, using a curvilinear grid with variable horizontal resolution [*Bentsen et al.*,
156 1999]. The mesh size was 1.4 km to the south and 0.8 km to the north. The southward decrease
157 in resolution was due to a compromise between the need to cover the western Mediterranean
158 basin at a reasonable cost, while considering the northward decrease of the Rossby radius, and
159 the need for increased resolution in the winter convection zone [*Estournel et al.*, 2016b]. Forty
160 vertical levels were used with closer spacing near the surface (15 levels in the first 100 m in the
161 center of the convection zone characterized by depths of ~2500 m).

162 The model was initialized and forced at its lateral boundaries with daily analyses provided by the
163 Mercator-Ocean operational system based on the NEMO model [*Maraldi et al.*, 2013]. The

164 configuration of this model was the PSY2V2R4 prototype based on the NEMO ocean modeling
165 platform and the SAM data assimilation system [Lellouche *et al.*, 2013] at a resolution of $1/12^\circ$
166 over the Atlantic and the Mediterranean from 20° S to 80° N. Following Estournel *et al.* [2016b],
167 the initial field and open boundary conditions were corrected from stratification biases deduced
168 from comparisons with observations taken during the MOOSE-GE cruise of August 2012.
169 Atmospheric forcing (turbulent fluxes) was calculated using the bulk formulae of Large and
170 Yeager [2004]. Meteorological parameters including downward radiative fluxes were taken from
171 the ECMWF (European Centre for Medium-Range Weather Forecasts) operational forecasts at
172 $1/8^\circ$ horizontal resolution and 3-hour temporal resolution based on daily analyses at 00.00 UTC.
173 River runoffs were considered based on realistic daily values for French rivers (data provided by
174 Banque Hydro, www.hydro.eaufrance.fr) and Ebro (data provided by SAIH Ebro,
175 www.saihebro.com) and mean annual values for the other rivers.



176

177 **Figure 1.** Location of the modeled area in the western Mediterranean Sea. The colored regions
178 correspond to the three regions considered in this study: the Deep Convection area (DCA,
179 yellow), Shallow Convection area (SCA, blue) and Stratified area (STA, green). Black dots on
180 the coastal band are river point-sources.

181 2.1.2 The biogeochemical model

182 The Eco3M-S model is a multi-nutrient and multi-plankton functional type model that simulates

183 the dynamics of the biogeochemical decoupled cycles of several biogenic elements (carbon,
184 nitrogen, phosphorus and silicon), and of non-Redfieldian plankton groups. The model structure
185 used in this study has been previously described in Ulises et al. [2016], Auger et al. [2011; 2014]
186 and Herrmann et al. [2013]. Most parameter values are based on the study of Ulises et al. [2016],
187 but a new calibration was carried out for some parameters using several observational datasets
188 [Kessouri et al., 2017].

189 The biogeochemical model was downscaled from the Mediterranean basin scale to the regional
190 scale described here. The biogeochemical basin scale model was forced by the temperature,
191 current and vertical diffusivity daily fields of the NEMO model (PSY2V2R4 analyses), which
192 was also used for the boundary conditions of our hydrodynamic model (Section 2.1.1). This
193 basin configuration was initialized in summer 2010, with climatological fields of nutrient
194 observations from the oligotrophic period in the Medar/ MedAtlas database [Manca et al., 2004].
195 Daily values of all state variables were extracted from the basin-scale run for the initial and
196 lateral boundary conditions of the regional model. This nesting protocol ensures the coherence of
197 the physical and biogeochemical fields at the open boundaries. The regional model was
198 initialized in August 2012. At the Rhone River mouth, nitrate, ammonium, phosphate, silicate
199 and DOC concentrations were prescribed using *in situ* daily data (P. Raimbault, personal
200 communication). These data, combined with those of Moutin et al. [1998] and Sempéré et al.
201 [2000], were used to estimate dissolved organic phosphorus and nitrogen, and particulate organic
202 matter concentrations as described in Auger et al. [2011]. At the other river mouths,
203 climatological values were prescribed according to Ludwig et al. [2010]. The deposition of
204 organic and inorganic matter from the atmosphere was neglected in this study. Benthic fluxes of
205 inorganic nutrients were considered by coupling the pelagic model with a simplified version of
206 the meta-model described by Soetaert et al. [2001]. The parameters of the latter model were set

207 following the modeling study performed by Pastor et al. [2011] for the Gulf of Lions shelf.

208 **2.2 MODIS satellite dataset**

209 Daily mean surface chlorophyll concentrations were extracted from the MODIS (Moderate
210 Resolution Imaging Spectroradiometer) Aqua (EOS PM) satellite dataset [*Ocean Biology*
211 *Processing Group*, 2014] for the period September 2012 to September 2013, in order to evaluate
212 the spatial and temporal variation of the modeled surface chlorophyll concentrations in the
213 western Mediterranean.

214 **2.3 Areas of study**

215 Temporal variations in the MLD are considered a major forcing of phytoplankton dynamics
216 [*Williams and Follows*, 2003]. In their study of the western Mediterranean, using a MLD dataset
217 and ocean color data, Lavigne et al. [2013] concluded that MLD plays a key role in
218 phytoplankton phenology, and can explain the coexistence of the two trophic regimes previously
219 observed [D'Ortenzio and Ribera d'Alcala, 2009]. A first regime in the northwestern convection
220 region is characterized by a deepening of the mixed layer in winter (reaching 1000 m for 52% of
221 the years for which observations were available between 1980 and 2013 [*Somot et al.*, 2016]),
222 followed by an intense phytoplankton bloom (similar to the subpolar regime [*Williams and*
223 *Follows*, 2003]). A second regime in the southern (Algerian) sub-basin is characterized by
224 continuous slow phytoplankton growth, concomitant with the shallow deepening of the mixed
225 layer (similar to the subtropical regime [*Williams and Follows*, 2003]). By analyzing the
226 interannual variability of satellite-derived surface chlorophyll, Mayot et al. [2016] distinguished
227 two sub-regimes in the northwestern convection region: bloom was found to be more
228 pronounced and delayed in the center of the convection zone than at its periphery. Mayot et al.
229 [2017a] showed that these two sub-regimes are distinguished by the intensity and duration of the

230 deepening of the mixed layer. Their study found that mean MLD exceeded 880 m for the central
231 “high bloom” region, over a period of one month, and reached 475 m, for a couple of days, in the
232 surrounding “bloom” region, in the winter of 2012/ 2013.

233 Following these earlier studies, we decided to divide the open-sea of the western Mediterranean
234 ($H > 1500$ m; H is the bathymetry) into three regions (Fig. 1), in order to carry out analyses of
235 phytoplankton dynamics and estimates of primary production and export. The first was the *Deep*
236 *Convection* region, defined as the area where daily average of MLD exceeded 1000 m for at least
237 one day during the studied winter. The second was the *Shallow Convection* region, defined as the
238 area in which daily average of MLD exceeded 150 m but did not reach 1000 m. The Shallow
239 Convection region was located at the periphery of the first area and mostly covered the Balearic
240 Sea. The third area, named the *Stratified* region, covered a large part of a deep pelagic zone in
241 the southwestern Mediterranean (Algerian sub-basin) where maximum winter MLD was less
242 than 150 m. In the present study, MLD was defined as the depth where potential density
243 exceeded the value at a depth of 10 m by 0.01 kg m^{-3} [Coppola et al., 2017]. This density-based
244 criterion (rather than a temperature-based criterion) avoids any overestimation of the MLD, and
245 any consideration of surface restratification caused by a change in surface heat flux, especially in
246 the deep convection region [Houpert et al., 2015]. The division into regions allowed us to focus
247 our analysis on the factors underlying differences in maximum winter MLD.

248 The heat fluxes, and hydrodynamic and biogeochemical variables that are presented in the
249 following sections correspond to the values of these variables averaged over all model grid
250 points included in the three areas. Furthermore, we calculated export below the regional
251 maximum photic zone at 150 m. Following Lazzari et al. [2012], this estimate of the depth of the
252 photic layer was based on the regional minimum value of the diffuse attenuation coefficient of
253 light at 490 nm derived from satellite observations (<http://marine.copernicus.eu/>), found close to

254 0.03 m^{-1} over the study period, and on the Lambert-Beer formulation to evaluate photosynthetic
255 available irradiance. Deep transfer was calculated at a depth of 800 m as, in general, temporal
256 variability in water masses at depths > 800 m is weak [Bethoux *et al.*, 1989]. Moreover, it is
257 possible that, in convection regions, deep waters below 800 m are mixed with overlying waters,
258 and a fraction of exported matter and its remineralization product are imported back into surface
259 and intermediate layers during the following winters. To discuss deep transfer on a longer period
260 than one year (Section 5.4), we also estimated export below the maximum MLD, as
261 recommended in Pavelsky *et al.* [2017]: this was computed at the greatest depth between 800 m
262 and the local maximum MLD over the study period, for each model grid point.

263 **2.4 Determination of bloom onset**

264 Understanding the environmental factors that control phytoplankton bloom onset has been a key
265 issue in a large number of studies [Siegel *et al.*, 2002; Behrenfeld, 2010; Brody and Lozier, 2015;
266 Henson *et al.*, 2009]. Several methods have been defined to determine its date. Siegel *et al.*
267 [2002] defined it as the first day of the year when surface chlorophyll concentration exceeds the
268 annual median, plus 5%. Adjustments to this method have been made to capture the subtropical
269 autumnal bloom, for instance, by considering the investigated year to start in September [Henson
270 *et al.*, 2009], or by avoiding consideration of a small, transient concentration increase by
271 changing the value of the threshold (10% instead of 5%, as in Bernardello *et al.* [2012]). Other
272 studies [Behrenfeld, 2010; Brody and Lozier, 2015] used observational data to develop a method
273 based on the net accumulation rate. The latter method is more appropriate to detect bloom onset
274 when the phytoplankton biomass is initially low [Brody *et al.*, 2013], as is the case in convective
275 regions. In the present study, bloom onset was considered as the day on which the net
276 accumulation rate of carbon biomass integrated through the water column (Eq. 1) exceeded 50%
277 of its annual maximum value.

$$r = \frac{\ln \frac{C(t+\Delta t)}{C(t)}}{\Delta t} \quad (1)$$

where r is the net accumulation phytoplankton rate, $C(t)$ is the depth-integrated phytoplankton biomass, and $\Delta t = 7$ days. The index r was compared to an index based on surface chlorophyll, using the method of Siegel et al. [2002], that we adapted for our study, by considering that the year began in September.

3. Model evaluation

A detailed validation of the coupled hydrodynamic and biogeochemical models over the study period is described in Estournel et al. [2016b] and Kessouri et al. [2017], respectively. Estournel et al. [2016b] conducted several comparisons with observations, such as the spatial distribution of water column stratification in winter at the scale of the northwestern sub-basin (their Fig. 6) or time series of the potential temperature profile in the center of the Gulf of Lions (their Fig. 11). In Kessouri et al. [2017], a comparison of the biogeochemical model results with nutrients and chlorophyll concentrations measured during the DeWEx winter and spring cruises was presented. This comparison showed that the model correctly reproduced the horizontal and vertical chlorophyll and nutrient distribution in these two seasons.

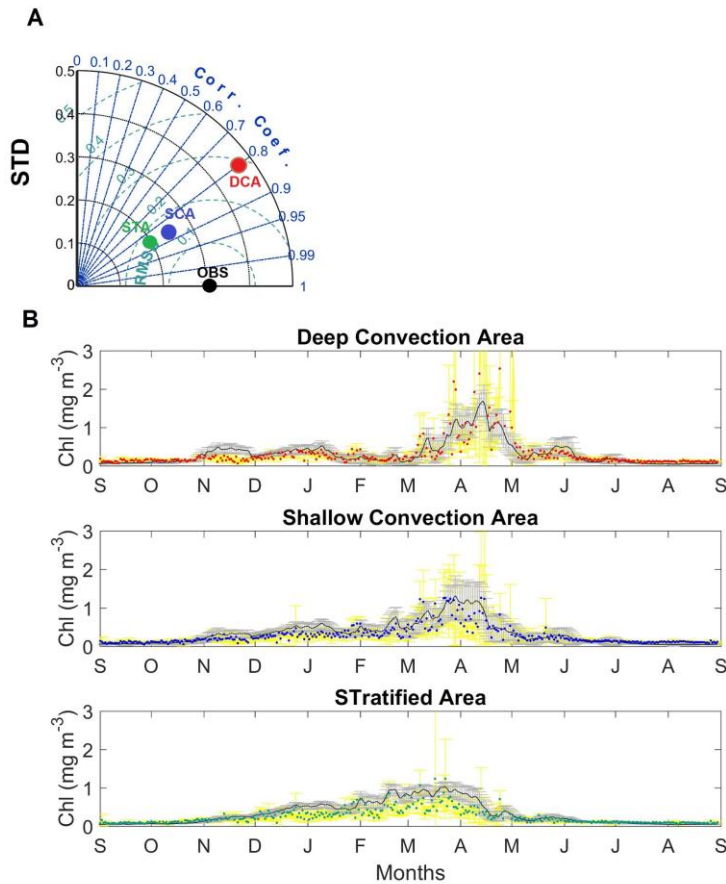
Here, the modeled seasonal evolution of surface chlorophyll in the three western Mediterranean regions (Deep Convection, Shallow Convection and Stratified) is compared with that derived from MODIS data over the period September 2012 to September 2013 (Fig. 2). Satellite data were interpolated on the model grid, then both modeled and observed chlorophyll were averaged in the three regions (model outputs corresponding to missing satellite data were not considered). Pearson correlations between surface modeled and satellite-derived chlorophyll concentrations were $R = 0.8, 0.85$ and 0.85 ($p < 0.01$) in the three regions, respectively (Fig. 2 upper panel). The

300 Nash-Sutcliffe efficiency (NS = 0.61, 0.55 and 0.2 respectively), indicated good-to-excellent
301 performance of the model according to Allen et al. [2007]. Mean biases represented a percentage
302 of the observed chlorophyll of -8% in the Deep Convection region, $+16\%$ in the Shallow
303 Convection region and $+30\%$ in the Stratified region. The temporal root mean square error was
304 maximum (0.26 mg m^{-3}) in the Deep Convection area (Fig. 2 upper panel) where the signal was
305 highly variable during bloom.

306 The timing of surface phytoplankton development and its magnitude were generally correctly
307 represented by the model in the three studied regions. The observations and the model exhibited
308 similar seasonal trends, that clearly show the contrast between the north and the south of the
309 basin: in February, concentrations increased from north to south, while in April this trend was
310 reversed. On the date of the maximum extent of the low chlorophyll area in the Deep Convection
311 region (February 19 according to model outputs, cloud-free images were too scarce to confirm
312 this), it covered the Gulf of Lions and Ligurian Sea (Fig. 1) in both model results and
313 observations (Fig. 3A and 3B). The spatial pattern of surface chlorophyll during the period of
314 maximum chlorophyll development (April 14) did not differ significantly between the model and
315 observations ($R = 0.58$ ($p < 0.01$)) (Fig. 3C and 3D). Spatial correlation in winter is higher
316 $R=0.8$).

317 Regarding the vertical distribution of chlorophyll in convection regions, Kessouri et al. [2017]
318 found a good agreement between model results and DeWEx cruise observations. Moreover, the
319 time evolution of the vertical distribution of phytoplankton in the Stratified (southern) region is
320 consistent with climatological observations reported by Lavigne et al. [2015]: the model
321 correctly reproduces the formation of a deep chlorophyll maximum (DCM) after the winter
322 mixing period and its deepening between 50 and 80 m in summer (presented in Section 4.2).

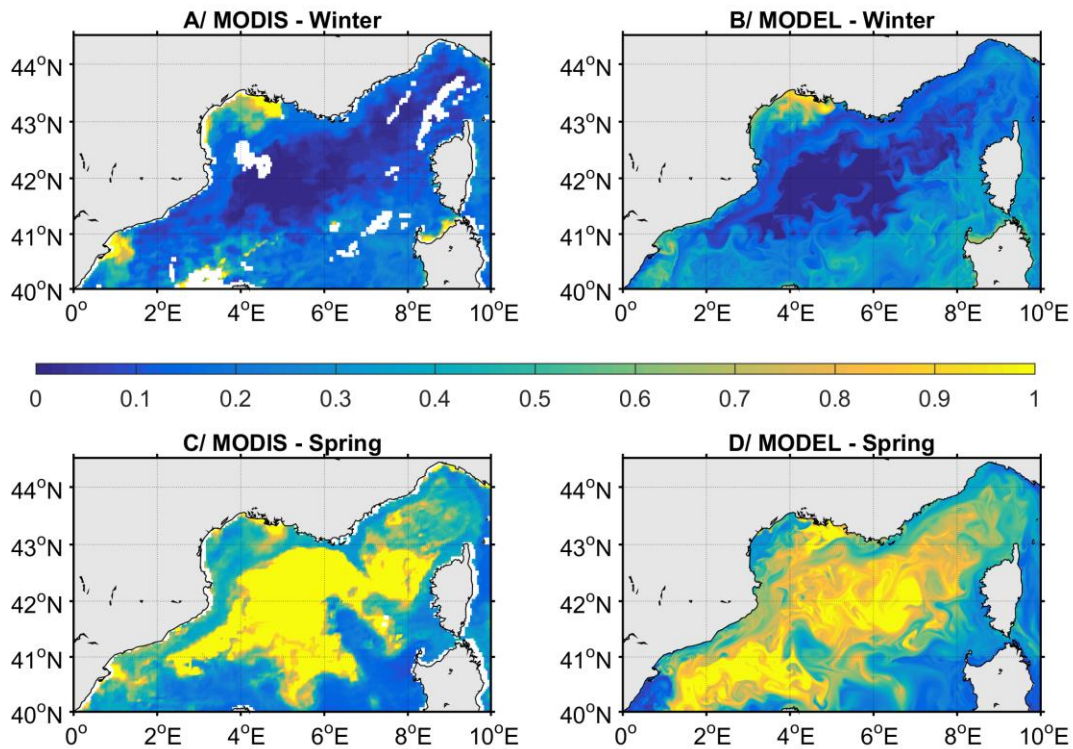
323 The evaluation of the model indicates that it reproduced the annual cycle of surface chlorophyll
 324 concentration in the three studied regions. However, it underestimated
 325 surface concentration in the Deep Convection region, and overestimated it in neighboring
 326 regions. Furthermore, the modeled vertical distribution was consistent with observations in the
 327 study area.



328
 329 **Figure 2.** (A) Taylor diagram comparing simulated and observed surface chlorophyll
 330 concentrations. OBS indicates MODIS data; DCA, SCA and STA indicate model outputs for the
 331 Deep Convection, Shallow Convection and Stratified regions, respectively. (B) Time series of

332 simulated (black line, median; gray bar, standard deviation) and observed (colored points and
 333 colored blue bars for standard deviation) surface chlorophyll concentrations (in mg m^{-3}) in the
 334 three regions: Deep Convection (DCA, red points), Shallow Convection (SCA, blue points) and
 335 Stratified (STA, green points) regions, from September 2012 to September 2013. Vertical dashed
 336 lines represent the dates of bloom onset (see Section 5.1 and Fig. 6).

337



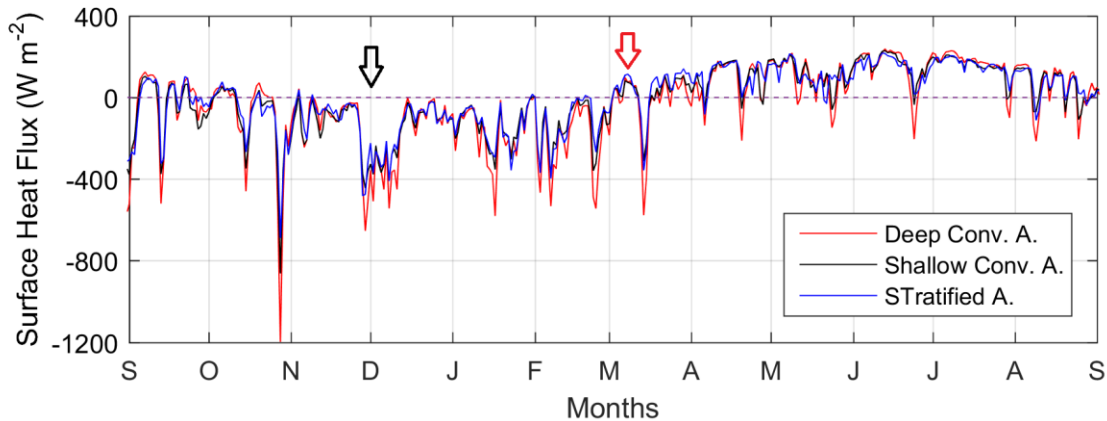
338

339 **Figure 3.** Comparison of simulated and MODIS chlorophyll concentrations (mg m^{-3}) in winter
 340 (19 February 2013, A and B) and spring (14 April 2013, C and D).

341 **4. Results**342 **4.1 Atmospheric conditions**

343 Intense cold and dry winds are an essential ingredient of deep convection. Using combined
344 atmospheric and oceanic observations, Estournel et al. [2016a] showed restratification of the
345 upper 500 m during periods of oceanic heat gain, generally associated with low wind conditions
346 and, conversely, the destruction (within hours) of an ocean stratification in response to the
347 passage of a continental air mass, associated with heat loss. Heat flux time series is therefore a
348 relevant parameter to consider in explaining variation in the MLD, which impacts the availability
349 of both nutrients and light for phytoplankton growth. A change in sign of surface heat fluxes can
350 also be used to detect bloom onset, as it induces a decrease in turbulent mixing, increasing the
351 time phytoplankton cells remain in the euphotic layer [Taylor and Ferrari, 2011].

352 The modeled heat flux evolution was similar in the three studied regions (Fig. 4). Temporal
353 correlation coefficients between heat fluxes in the Shallow Convection and Deep Convection
354 regions, and between the Stratified and Deep Convection regions, were significant at 0.96
355 ($p < 0.01$) and 0.93 ($p < 0.01$), respectively. Each region was characterized by a major heat loss
356 between September 2012 and mid-March 2013, and a heat gain from mid-March 2013 to
357 September 2013. However, there were clear differences in its magnitude for the three regions.
358 Specifically, heat losses were higher in the Deep Convection region, which is directly exposed to
359 the Mistral and Tramontane winds, than in the two other regions. In this region, average of
360 winter heat flux was -180 W m^{-2} , compared to -140 W m^{-2} in the Shallow Convection region
361 and -130 W m^{-2} in the Stratified region. Heat loss exceeded 400 W m^{-2} eleven times in the Deep
362 Convection region from September 2012 to March 2013, while it only exceeded this value twice
363 in the two other regions.



364

365 **Figure 4.** Time series of spatially averaged heat flux (W m^{-2}) calculated for the three studied
 366 regions: Deep Convection is shown in red, Shallow Convection in blue, and Stratified in
 367 green. The dates of bloom onset are indicated by arrows (in black for autumn bloom, in red
 368 for spring bloom, see Section 5.1).

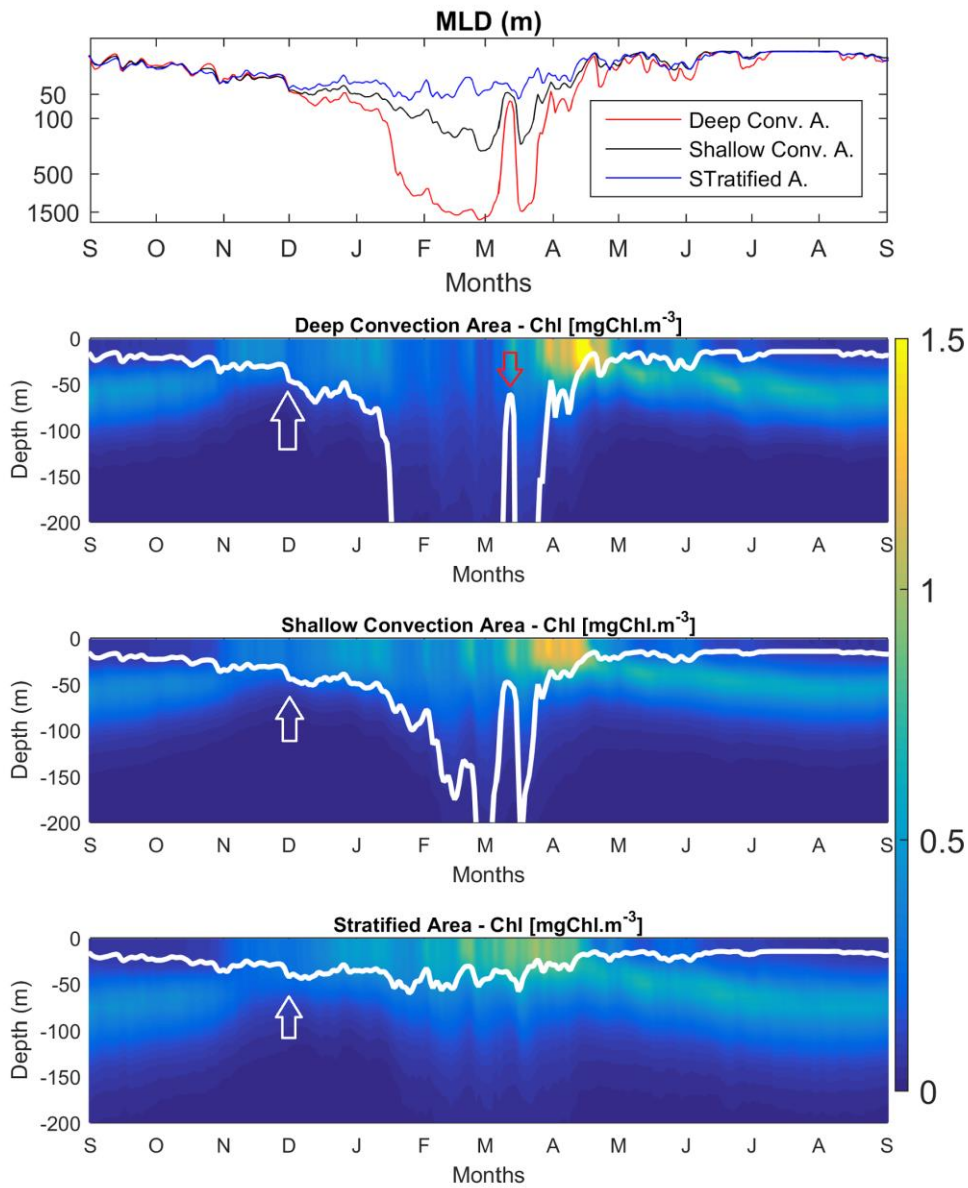
369 4.2 Temporal variability of MLD and chlorophyll concentration

370 Figure 5 presents the time evolution of the modeled MLD, spatially averaged for the three
 371 regions. The mixed layer deepened progressively from October to January, and then more
 372 abruptly from January to March. Despite a few events, characterized by low surface heat loss,
 373 that interrupted this deepening, it reached maximum values of 1900 m in the Deep Convection
 374 region, 260 m in the Shallow Convection region and 60 m in the Stratified region at the end of
 375 February. During the first week of March, which was characterized by positive surface fluxes,
 376 significant restratification due to surface and intermediate waters advection was observed
 377 [Estournel *et al.*, 2016a]. This led to mixed layer shoaling in the Deep and Shallow convection
 378 regions. However, this stratification was insufficient to withstand mid-March gusty winds, which
 379 further deepened the mixed layer. After this last deep mixing event, stratification became stable,

380 marking the end of winter.

381 The three regions were broadly similar in terms of their chlorophyll dynamics, the exception
382 being winter. A DCM was observed in spring, summer and autumn in the three regions. DCM
383 formation was earlier in the Stratified region (mid-April) than in the Shallow Convection (end of
384 April) and in Deep Convection (May) regions. From its formation, DCM deepened until August,
385 when it reached 60–70 m. In autumn, it became shallower as the light intensity reduced.
386 Chlorophyll concentrations in the DCM decreased from the time of the DCM formation in
387 spring, until its disappearance in November. An intense wind event and heat loss at the end of
388 October deepened the mixed layer, which reached the DCM and led to its disappearance by
389 dilution (discussed in Section 5.1.1). During the second half of December, surface chlorophyll
390 concentration increased considerably.

391 From mid-January to early March, several wind gusts interrupted surface phytoplankton
392 development in all three regions, but the duration and frequency of these interruptions varied
393 from one region to another. For example, in the Deep Convection region, surface chlorophyll
394 concentrations decreased significantly in response to deep mixing, whereas in the Stratified
395 region, the decrease was smaller and was concentrated into short periods (Fig. 5). From the end
396 of March to mid-April, all three regions were characterized by a sustained increase in surface
397 chlorophyll concentration. A comparison of the regions suggests that strong mixing delayed the
398 biomass increase (discussion in Section 5.1). Moreover, surface phytoplankton development was
399 shorter and more intense where mixing was deep. For instance, in the Deep Convection region, it
400 lasted about 1.5 months with chlorophyll concentrations above 1.5 mg m^{-3} during the bloom. In
401 the Stratified region, it lasted at least 2.5 months, with chlorophyll values remaining below 1 mg
402 m^{-3} .



404 **Figure 5.** The top panel represents the temporal evolution of the simulated MLD (m) in the Deep
405 Convection region (red), the Shallow Convection region (blue), and the Stratified region (green)
406 from September 2012 to September 2013. The y-axis is logarithmic. The other panels represent
407 average chlorophyll concentration (mg m^{-3}) for each of the studied regions (Deep Convection,
408 Shallow Convection and Stratified region, from upper to lower panels, respectively). The MLD
409 is superimposed (white line). Arrows indicate bloom onset (in white for autumn bloom, in red for
410 spring bloom, see Section 5.1).

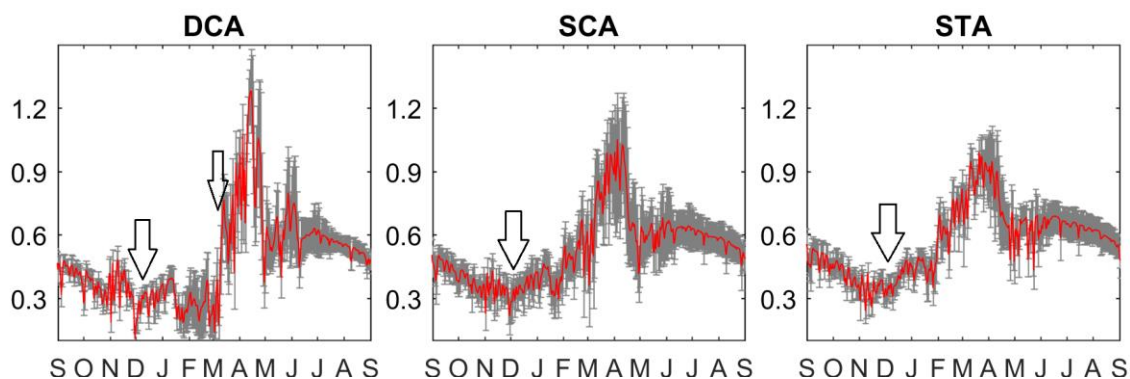
411 **4.3 Primary production**

412 In winter (December–February), the modeled, vertically integrated net primary productivity
413 (NPP) (Fig. 6) had a mean and standard deviation of 0.45 ± 0.09 and $0.55 \pm 0.13 \text{ gC.m}^{-2} \text{ day}^{-1}$ in
414 the Shallow Convection and Stratified regions, respectively: both NPP means were higher than in
415 the Deep Convection region (mean $0.3 \text{ gC m}^{-2} \text{ day}^{-1}$). NPP increase began in February in the
416 Shallow Convection and Stratified regions, and one month later in the Deep Convection region.
417 NPP reached its maximum in all three regions in spring (mean \pm standard deviation of $0.91 \pm$
418 0.21 , 0.86 ± 0.13 , and $0.8 \pm 0.10 \text{ gC m}^{-2} \text{ day}^{-1}$ in the Deep Convection, Shallow Convection and
419 Stratified regions, respectively). A secondary peak (higher in the Deep Convection region than in
420 the two other regions) occurred between mid-May and early June. From early June to November,
421 NPP slowly decreased, with average values of $0.5 \pm 0.05 \text{ gC m}^{-2} \text{ day}^{-1}$ in the three studied
422 regions.

423 This seasonal evolution of NPP is consistent with earlier results based on *in situ* observations
424 using the ^{14}C method in the Ligurian Sea [*Marty and Chiavérini, 2002*] and remote sensing in
425 various regions of the Mediterranean basin [*Bosc et al., 2004; Uitz et al., 2012*]. However,
426 summer NPP was higher in the model ($0.6 \text{ gC m}^{-2} \text{ day}^{-1}$) than for observations ($0.4 \text{ gC m}^{-2} \text{ day}^{-1}$),

427 especially in the Shallow Convection and Stratified regions. This summer overestimation has
428 also been identified for other numerical models [*Crispi et al.*, 2002; *Allen et al.*, 2002; *Lazzari et*
429 *al.*, 2012]. These differences could be nuanced by limitations in the determination of primary
430 production based on remote sensing in the presence of a DCM, as most of the light recorded by
431 remote sensing emanates from the upper few centimeters of the water column [*Helbling and*
432 *Villafane*, 2009]. The impact of this limitation on the estimate of annual primary production
433 could be all the more significant following the work of *Macias et al.* [2014], who estimated that
434 primary production in the DCM represents 62% of the total primary production in the open-sea
435 Mediterranean regions. The results of our model showed that 90% of primary production in
436 spring/ summer, and 70% at the beginning of the fall occurred in the DCM layer in all three
437 regions.

438 At the annual scale, we estimated a NPP of $175 \pm 6 \text{ gC m}^{-2} \text{ year}^{-1}$ in the Deep Convection region,
439 $192 \pm 14 \text{ gC m}^{-2} \text{ year}^{-1}$ in the Shallow Convection region, and $207 \pm 14 \text{ gC m}^{-2} \text{ year}^{-1}$ in the
440 Stratified region. Because of the overestimation of surface chlorophyll in the Stratified region,
441 and the underestimate in the Deep Convection region, we did not consider the inter-region NPP
442 trend significant. By way of comparison, *Lazzari et al.* [2012] did not observe any clear NPP
443 gradient between the eastern Algerian sub-basin and the northwestern region, based on a coupled
444 physical-biogeochemical model.



445
 446 **Figure 6.** Time series from September 2012 to September 2013 of simulated net primary
 447 production (NPP) ($\text{gC m}^{-2} \text{ day}^{-1}$) spatially averaged (red) and standard deviation (gray) in the
 448 Deep Convection (DCA, left), Shallow Convection (SCA, middle) and Stratified (STA, right)
 449 regions. Vertical arrows indicate bloom onset (See Section 5.1).

450 4.4 POC and DOC export

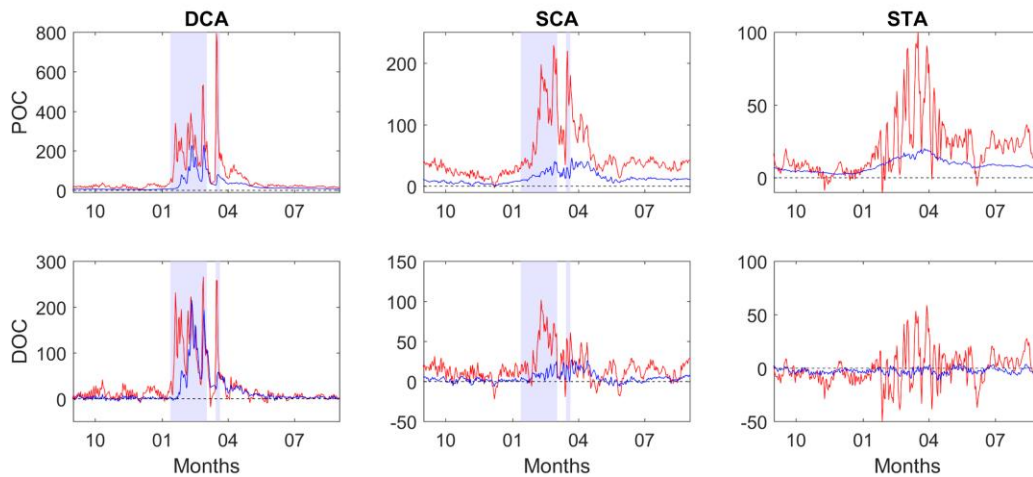
451 Figure 7 presents the time evolution of the modeled export of DOC and POC at 150 and 800 m
 452 depths. This was calculated as the net downward flux induced by turbulent mixing, advection
 453 and sedimentation (for particulate matter). In summer and autumn, vertical export was low in all
 454 three regions. In the Deep Convection region, where the MLD reached at least 500 m between
 455 mid-January and the first week of March (Fig. 5), POC and DOC fluxes were strong and
 456 variable, with peaks coinciding with strong mixing events (mid-January, beginning and end of
 457 February, and mid-March, see Fig. 4). During the main convection event, the export at 150 (800)
 458 m reached 0.6 (0.2) $\text{gC m}^{-2} \text{ day}^{-1}$ for POC, and 0.25 (0.2) $\text{gC m}^{-2} \text{ day}^{-1}$ for DOC. During the
 459 secondary convection event (the third week of March), simulated export is characterized by a
 460 high peak at 150 m (0.95 $\text{gC m}^{-2} \text{ day}^{-1}$ for POC, and 0.30 $\text{gC m}^{-2} \text{ day}^{-1}$ for DOC), with another
 461 moderate peak at 800 m (0.06 and 0.05 $\text{gC m}^{-2} \text{ day}^{-1}$ for POC and DOC, respectively). Similarly,

462 in the Shallow Convection region, POC and DOC export was maximum during mixing events,
463 exceeding $0.15 \text{ gC m}^{-2} \text{ day}^{-1}$ and $0.05 \text{ gC m}^{-2} \text{ day}^{-1}$, respectively, at 150 m (compared to 0.02 gC
464 $\text{m}^{-2} \text{ day}^{-1}$ and $0.02 \text{ gC m}^{-2} \text{ day}^{-1}$, respectively, at 800 m). In both convection regions, an increase
465 of POC and DOC export was simulated at 150 m in April during bloom. In the Stratified region,
466 POC export at both depths was maximum during mixing periods, notably the period coinciding
467 with maximum phytoplankton development (when it reached 0.10 and $0.02 \text{ gC m}^{-2} \text{ day}^{-1}$). DOC
468 export at 150 m was highly variable (positive and negative peaks reaching $0.05 \text{ gC m}^{-2} \text{ day}^{-1}$),
469 especially in winter; it was much lower at a depth of 800 m for the whole year.

470 At the annual scale (Table 1), modeled POC and DOC export at both depths followed the same
471 increasing trend: it was higher in regions where vertical mixing was deeper. The spatial mean
472 and standard deviation of export at 150 (800) m were estimated at 25 ± 34 (8 ± 9), 15 ± 14 ($4 \pm$
473 6) and 8 ± 6 (3 ± 4) $\text{gC m}^{-2} \text{ year}^{-1}$ for POC, and 10 ± 17 (5 ± 7), 5 ± 6 (1 ± 1.5) and -1 ± 5 ($-2 \pm$
474 3) $\text{gC m}^{-2} \text{ year}^{-1}$ for DOC, in the Deep Convection, Shallow Convection and Stratified regions,
475 respectively. It is noteworthy that spatial variability was high within each region. The influence
476 of convection on annual export will be discussed in Section 5.2. and the efficiency of export and
477 transfer to deep waters in Section 5.3. The deep transfer of organic carbon and the comparison of
478 the three regions on a decadal timescale will be discussed in Section 5.4.

479 The simulated seasonal evolution of POC export below the photic zone agrees with sediment trap
480 measurements from the DYFAMED station in the Ligurian Sea (Fig. 1) [Miquel *et al.*, 2011] and
481 the LION site in the Gulf of Lions (Fig. 1) [Stabholz *et al.*, 2013]. Both indicated: (1) rapid
482 exports of particulate and dissolved matter during convection; (2) a bloom-induced export in
483 spring; and (3) low export rates during the stratified period. From a quantitative point of view,
484 Gogou *et al.* [2014] estimated an annual flux of $23 \text{ gC m}^{-2} \text{ year}^{-1}$ at 100 m at the LION site
485 (Fig.1); Miquel *et al.* [2011] found an annual flux of $2.5 \text{ gC m}^{-2} \text{ y}^{-1}$ at 200 m at DYFAMED; and

486 Zúñiga et al. [2007] reported an annual flux of $\sim 6 \text{ gC m}^{-2} \text{ year}^{-1}$ at 250 m in the Algerian sub-
 487 basin (Point A on Fig 1). At the same locations and depths, our model estimated annual POC
 488 fluxes of 52, 19 and $11 \text{ gC m}^{-2} \text{ year}^{-1}$, respectively. The higher POC fluxes obtained in the
 489 convection regions in the model may be partly explained by an underestimation of POC export
 490 from sediment trap measurements during intense mixing periods [Buesseler et al., 2007].
 491 Regarding DOC export, our estimate of $18 \text{ gC m}^{-2} \text{ year}^{-1}$ is similar to measurements carried out
 492 by Copin-Montégut and Avril [1993] and Avril [2002] of 18 and $12 \pm 6 \text{ gC m}^{-2} \text{ year}^{-1}$,
 493 respectively, at 100 m in the Ligurian Sea. The annual POC flux at mid-depth has been estimated
 494 in observational studies at the LION site as 2.4 and $1.9 \text{ gC m}^{-2} \text{ year}^{-1}$ at 1000 m [Stabholz et al.,
 495 2013; Gogou et al., 2014]. This can be compared to $1.6 \text{ gC m}^{-2} \text{ year}^{-1}$ at 1000 m at DYFAMED
 496 [Miquel et al., 2011], and $4.8 \text{ gC m}^{-2} \text{ year}^{-1}$ at 845 m in the Algerian sub-basin [Zúñiga et al.,
 497 2007]. At the same locations and depths, the model computed sedimentation export of 2.8, 2.6
 498 and $3.1 \text{ gC m}^{-2} \text{ year}^{-1}$, respectively, which is close to observations.



499

500 **Figure 7.** Time series from September 2012 to September 2013 of modeled particulate (upper
 501 panel) and dissolved (lower panel) organic carbon export ($\text{mgC m}^{-2} \text{ day}^{-1}$) at 150 m depth (in red)

502 and 800 m (in blue), in the Deep Convection Area (DCA, left), Shallow Convection Area (SCA,
503 middle) and Stratified Area (STA, right). The first blue bar corresponds to the main convection
504 event, and the second blue bar represents the short deep mixing event of the third week of
505 March.

506 **5. Discussion**

507 **5.1. Conditions favoring bloom onset**

508 ***5.1.1. Autumnal bloom***

509 As described in Section 2.4, we determined bloom onset based on the net accumulation rate of
510 phytoplankton biomass. The autumnal bloom onset occurred at the beginning of December in the
511 two convective regions, and a few days later in the Stratified region (red vertical dashed lines in
512 Fig. 8). This difference is not significant, as it is sensitive to the choice of the threshold for the
513 rate of accumulation (especially in the Stratified region). The following analysis concerns the
514 early December period for the three regions.

515 Atmospheric forcing, biotic and abiotic conditions at the onset of the autumnal bloom were
516 similar in the three regions: (1) bloom was triggered during a period of high heat losses (Fig. 8b,
517 8h, 8n); (2) the mixed layer suddenly deepened (40–50 m in the three regions, Fig. 8c, 8i, 8o);
518 (3) turbulent diffusivity suddenly increased in all regions (Fig. 8d, 8j, 8p); (4) zooplankton
519 integrated biomass constantly decreased after September (Fig. 8e, 8k, 8q); and (5) nitrate and
520 phosphate concentrations at the surface began to increase in all regions: concentrations reached 2
521 mmol m^{-3} and $> 0.1 \text{ mmol m}^{-3}$, respectively, in the Deep Convection region, about two times
522 lower in the Shallow Convection region, and four times lower in the Stratified region, while they
523 had been close to 0 prior to the bloom triggering (Fig. 8f, 8l, 8r).

524 An estimate of bloom onset based on surface chlorophyll, rather than vertically integrated
525 organic carbon would have brought it forward by one month (Fig 8, dashed black lines). The
526 increase of surface chlorophyll at the end of October was caused by the erosion of the DCM, at a
527 time when the mixed layer deepened, without reaching the nutricline. This purely physical
528 process was not accompanied by an increase in integrated carbon (red solid line in Fig 8a, 8g,
529 8m) and was therefore not considered as bloom within the meaning of integrated biomass
530 increase. It should be noted that the corollary of this process is a potential bias in remote sensing
531 detection of post-DCM bloom. The period between the two estimates (based on surface
532 chlorophyll and vertically integrated biomass) corresponds to the increase in the MLD from the
533 DCM to the nutricline. In our case, this period lasted one month, which appears long if we
534 consider the proximity of the DCM to the nutricline (about 20 m, see Kessouri et al. [2017]).
535 However, in the present case, it corresponded to the period between two strong wind and heat
536 loss events at the end of October and the end of November (Fig. 4), each of which coincided with
537 a sudden deepening of the mixed layer (see Estournel et al. [2016b] their Fig. 11 for the
538 temperature evolution in the 150-m upper layer). The first event deepened the mixed layer down
539 to the DCM, and the second brought it below the nutricline. This sequence of events, which
540 began with the mixing of the DCM, followed by an increase of primary production caused by the
541 nutrient supply from deeper layers, induced by increased wind stress, has been previously
542 described by Chiswell et al. [2013]. Lavigne et al. [2015] indicated that DCM erosion could
543 explain 60% of chlorophyll profiles observed in the Ionian region in December and January.

544 The triggering of the autumn bloom corresponds to the description by Williams and Follows
545 [2003] of the subtropical bloom onset, which occurs when the deepening mixed layer provides
546 new nutrients (Fig. 9). However, we noted that the integrated zooplankton biomass was low in all
547 three regions at autumn bloom onset (reaching a minimum in the Shallow Convection and

548 Stratified regions). Therefore, it is likely that the low magnitude of grazing pressure participated
549 to trigger the autumn bloom [Behrenfeld *et al.*, 2010; Behrenfeld and Boss, 2014]. Moreover, we
550 noted that the ongoing mixed layer deepening following the autumn bloom induced dilution,
551 which prevented the zooplankton biomass taking advantage of the autumn bloom to grow in the
552 Deep Convection region.

553

554 ***5.1.2. Winter/ early spring bloom in the Deep Convection area***

555 In the Deep Convection region, the autumnal bloom was interrupted for a period of two months
556 (from mid-January to mid-March) due to a lack of light that was, in turn, due to deep mixing. In
557 February, the patch of chlorophyll was vertically homogeneous with a surface chlorophyll
558 concentration below $0.1 \text{ mg Chl m}^{-3}$ (Fig. 3a and 5a) and high nutrient concentrations
559 ($> 7 \text{ mmol N m}^{-3}$ and $> 0.3 \text{ mmol P m}^{-3}$) [Kessouri *et al.*, 2017]. The vertically integrated
560 phytoplanktonic biomass was almost constant (Fig. 8a). Winter/ early spring bloom onset was
561 identified in the Deep Convection region on March 8. The conditions that triggered it differed
562 from those that triggered autumnal bloom. Specifically, the former started after a few days of
563 positive heat flux (Fig. 8b), when vertical turbulence decreased significantly (Fig. 8d) and the
564 mixed layer became abruptly shallower (100 m, Fig. 8c). Nitrate and phosphate surface
565 concentrations were high, with values $> 6.5 \text{ mmol m}^{-3}$ and $> 0.25 \text{ mmol m}^{-3}$, respectively (Fig.
566 8f), while zooplankton biomass and grazing rate reached their annual minimum (Fig. 8e).

567 These results (summarized in Fig. 9) are consistent with the analysis of the triggering of the
568 North Atlantic subpolar bloom by Williams and Follows [2003], and the results of Taylor and
569 Ferrari [2011] obtained from analytical theory and high-resolution numerical simulations. Both
570 studies emphasized the role of positive (or the reduction of negative) surface heat fluxes. The

571 simultaneous breakdown of turbulence and a decrease in MLD means that our results also
572 support the discussion of Brody et al. [2013], who argued that a change in sign of heat flux is not
573 the only factor that could restratify the mixed layer, horizontal advection being another. For
574 example, restratification could occur in response to horizontal advection by mixed layer eddies,
575 as shown by Mahadevan et al. [2012], based on observations in the North Atlantic.

576 The work of Estournel et al. [2016b] showed that, based on a heat and salt budget in the
577 convection zone, from December, horizontal advection acted to stratify the surface layer, with a
578 sustained warming trend that opposed the effect of surface heat fluxes. They reported that during
579 a period of light winds (the beginning of March), the heat budget became positive in surface and
580 intermediate layers. This was argued to be due to the fact that the front between the convective
581 dense layer and adjacent light water became baroclinically unstable, producing restratification by
582 advection of warm water inside the mixed patch.

583 Following these authors, it is clear that restratification is intrinsically linked to the change in sign
584 of surface fluxes (or the fall of negative fluxes) as baroclinic instability develops when surface
585 heat losses decrease and no longer maintain the verticality of isopycnals. This suggests that the
586 bloom was indirectly triggered by the decline in surface heat losses, which induced a conjunction
587 of closely-related effects: the breakdown of turbulence and water column restratification.
588 However, it should be noted that these arguments were based on a spatial average over a
589 relatively wide, and very heterogeneous area. It is probable that if each point of the model is
590 examined, processes would be more differentiated. For example, the main impact of
591 restratification induced by frontal instabilities should have been at the perimeter of the domain,
592 whereas the 1D turbulence breakdown process was probably more effective in the center of the
593 convective patch. Although a study of these coupled, submesoscale processes is beyond the
594 scope of this paper, it deserves dedicated examination.

595 Our results also illustrate that the decoupling of phytoplankton and grazers during the winter
596 period was another factor that favored phytoplankton growth after bloom onset. It is of note that
597 small positive and negative changes in the integrated phytoplankton biomass in winter (from
598 December to the spring bloom onset) were associated with the beginning and end of windy
599 conditions and induced heat flux, and uncorrelated with variations in grazing pressure. This
600 indicates that prey–predator decoupling was strong throughout the winter (phytoplankton
601 development being mostly related to mixing-induced nutrient supply). As Behrenfeld and Boss
602 [2014] describe, recoupling is slow, as phytoplanktonic concentration must increase to stimulate
603 grazing and encourage a subsequent increase in herbivores. This recoupling condition was not
604 met during winter, and this explains the continuous decrease of zooplanktonic biomass, which
605 only recovered when phytoplankton rapidly accumulated during the spring bloom as a result of
606 the hydrodynamic factors discussed above.

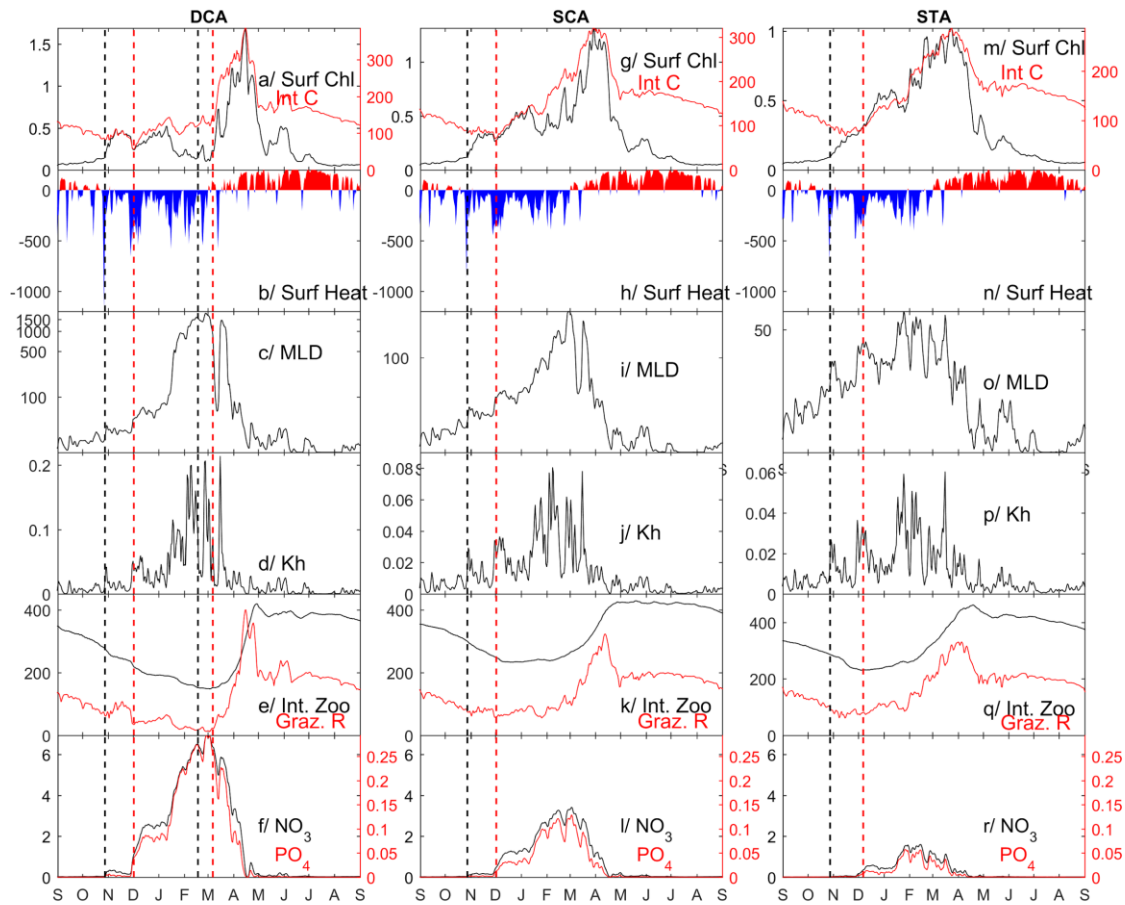
607 Our results for the northwestern Mediterranean are consistent with those of Bernardello et al.
608 [2012], who found that bloom started as vertical mixing decreased, generally in mid-March.
609 They are also consistent with an observational study by D’Ortenzio et al. [2014] who reported
610 that, in the deep convection region, the triggering of the bloom was unrelated to a change in the
611 nutrient stocks of the euphotic layer since this stock was already available three months before
612 onset. Finally, Auger et al. [2014] found a negative correlation between convection intensity and
613 winter zooplankton biomass; this finding confirms the hypothesis that phytoplankton
614 zooplankton decoupling induced by convection favors the explosion of the phytoplankton
615 biomass.

616 ***5.1.3. Phytoplankton growth in the Shallow Convection and Stratified regions***

617 In the Stratified region, no new bloom onset was identified during the months that followed the

618 autumn bloom, while the vertically integrated biomass progressively increased. This is a
619 characteristic of the subtropical region. In our results, after the autumn bloom, sustained winter
620 mixing supplied nutrients almost continuously, producing a moderate accumulation of
621 phytoplankton that was controlled by herbivores whose biomass was low, but which remained at
622 a higher level than in the Deep Convection region.

623 The method based on accumulation rates identified several blooms in the Shallow Convection
624 region in winter (not shown). Biomass increases corresponded to short, calm periods (heat gain
625 or low heat loss), and were followed by long periods of slow growth that resembled those of the
626 Stratified region. It is likely that this behavior was specific to the particular year studied. Indeed,
627 during the study period, the mixed layer remained relatively undeveloped for a long time, not
628 exceeding 150 m in depth until the end of February (Fig. 8i). Finally, findings for the Shallow
629 Convection region lay between the other two regions (Fig. 9). Like the Stratified region, the
630 increase in integrated biomass was progressive but, like the Deep Convection region, surface
631 chlorophyll increased rapidly in March/ April. The grazing time series was more similar to that
632 of the Stratified region than the Deep Convection region.



633

634 **Figure 8.** Time series from September 2012 to September 2013 of (a, g, m) modeled depth-
 635 integrated phytoplankton biomass ($mgC m^{-2}$) in red and surface chlorophyll concentration
 636 ($mmol.m^{-3}$) in black, (b, h, n) net heat flux ($W m^{-2}$) with heat losses in blue and heat gains in red,
 637 (c, i, o) MLD (m), (d, j, p) the 0–75 m averaged turbulent diffusivity ($m^2 s^{-1}$), (e, k, q) depth-
 638 integrated zooplankton biomass in black ($mgC m^{-2}$) and grazing rate in red ($mgC m^{-2} day^{-1}$), and
 639 (f, l, r) nitrate (in black) and phosphate (in red) surface concentrations ($mmol.m^{-3}$), in the Deep
 640 Convection area (DCA, left), the Shallow Convection area (SCA, middle) and the Stratified area

641 (STA, right). Vertical dashed lines indicate the dates of bloom onset (black = using surface
642 chlorophyll concentrations; red = using the vertically integrated biomass, see Section 2.4).

643 **5.2 Influence of convective mixing on organic carbon export**

644 Organic carbon is exported under the productive layer through two main mechanisms:
645 (1) sedimentation, which only involves individual or aggregated particles with a sufficiently high
646 settling velocity compared to their rate of decomposition and remineralization; and (2) vertical
647 mixing and advection that affect all organic carbon. Observations of the DeWEx Leg1 campaign
648 in February 2013 showed the presence of phytoplankton at depths > 2000 m, at concentrations of
649 0.16 mg m^{-3} [Kessouri *et al.*, 2017]. These observations suggest that vertical mixing and
650 advection are responsible for the presence of organic carbon, including light cells and detritus, in
651 deep layers, as observed by Giering *et al.* [2016] in the Iceland Basin, and modeled by Ulses *et*
652 *al.* [2016] in the northwestern Mediterranean. It is likely that a fraction of the exported matter
653 observed in deep waters during the winter of 2012/ 2013 was permanently trapped when mixing
654 stopped.

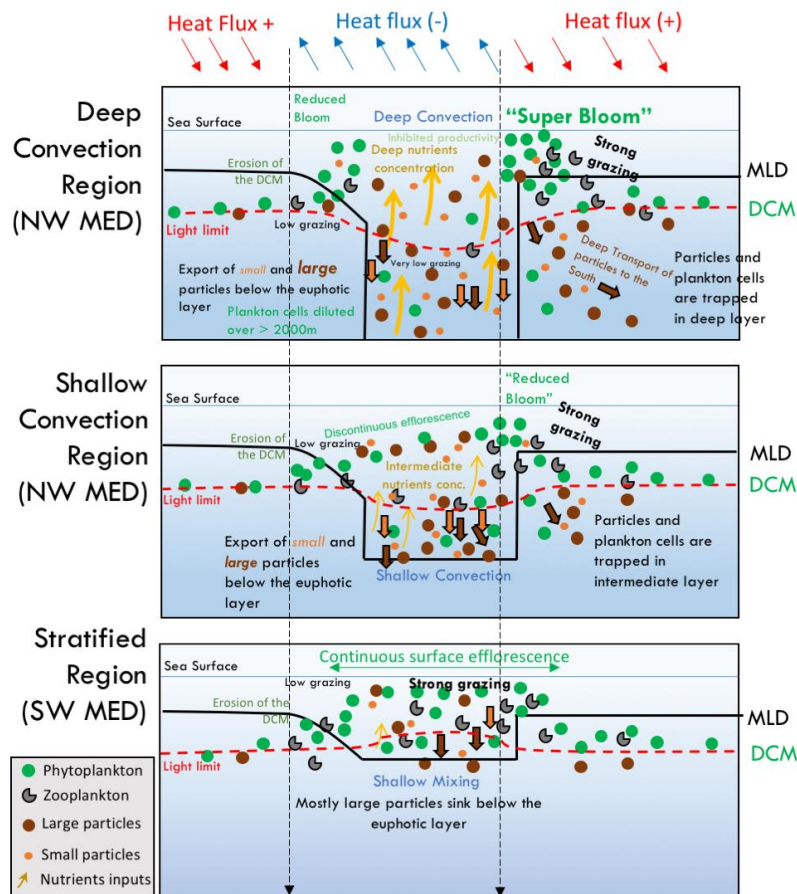
655 Our model reproduces the homogenization of chlorophyll throughout the mixed layer during
656 convective events, shown by a comparison of the model's results with DeWEx cruise
657 observations performed by Kessouri *et al.* [2017] (see their Fig. 3). Our findings show that the
658 net export fluxes of POC and DOC at 150 m are more than six times higher during these events
659 than during the rest of the year (Fig. 7). The first convection event (15 January to 7 March) took
660 place after the autumnal bloom (Section 5.1). In the Deep Convection region, POC and DOC
661 exports during this event constituted 48 and 61%, respectively, at 150 m, and 50 and 66%,
662 respectively, at 800 m, of the annual amount. The percentages were lower in the Shallow
663 Convection region: 32% and 39% for the export of POC and DOC, respectively, at 150 m (21
664 and 24%, respectively, at 800 m).

665 The secondary convection episode lasted 9 days, from 15 to 23 March 2013, and followed a
666 period of weak stratification during which the winter/ early spring bloom began (Section 5.1). In
667 the Deep Convection region, the export of POC and DOC integrated on this secondary event
668 represented 12 and 9% at 150 m (6 and 7% at 800 m) of the respective annual export. This can
669 be compared to the Shallow Convection region, with 8% and 6% at 150 m (6 and 11% at 800 m).

670 Intermittent convection was observed by Houpert et al. [2016] based on mooring data in the
671 center of the Gulf of Lions, with a secondary deep convection event occurring in March, each
672 year from 2009 to 2013. The model revealed the importance of this recurrent characteristic on
673 the annual export of organic matter. It appears an alternation of periods of restratification, that
674 favors phytoplankton growth, and vertical mixing, that entrains a fraction of new biomass under
675 the euphotic layer. This phenomenon could explain the different peaks in POC and DOC export
676 modeled in mid-January, the beginning and end of February, and the third week of March in
677 convection regions. These peaks corresponded to peaks in heat loss at the ocean surface (Fig. 4)
678 that triggered convection.

679 The importance of this “mixed layer pump” mechanism [*Gardner et al.*, 1995], which is very
680 clear in the present study period, has been reported in other studies. Bernardello et al. [2012]
681 showed that the frequency of gales during the bloom period was a determining factor in the
682 interannual variability of export in the deep convection region of the northwestern
683 Mediterranean. In other regions, Bishop et al. [1986] estimated that 67% of primary produced
684 carbon was removed by convective mixing during a transient stratification period in a warm-core
685 ring in the northwest Atlantic. Similarly, Ho and Marra [1994] found that a large amount of
686 newly produced organic carbon was exported by mixing during a transient stratification period in
687 the northeast Atlantic. In their study of a shallow convection region in the North Atlantic and
688 equatorial Pacific, Gardner et al. [1995] reported the importance of the deepening of the mixed

689 layer at night, which favored the new production during the day and export of organic carbon
 690 produced. Koeve et al. [2002] estimated that vertical mixing associated with storms, which
 691 interrupted the beginning of the early spring bloom, contributed to the export of a large fraction
 692 of seasonal new production (between 56% and 65% in 1992, and about 36% in 1989) in the
 693 northeast Atlantic.



694

695 **Figure 9:** Conceptual model representing plankton and particles behavior for three different

696 regimes in the western Mediterranean Sea. This conceptual model resumes the various sequences
697 from the destruction of the DCM, the injection of nutrients to the euphotic layer, the deep mixing
698 of the living cells (in the 1st region), the triggering of the blooms and the new setting up of the
699 DCM affected by different strength mixing. These sequences are shown simultaneously with
700 different ways of small and large organic particles export and trapping below the euphotic layer
701 via the mixing layer pump.

702 **5.3 Efficiency of the export of organic carbon and transfer to the deep layer**

703 Table 1 presents the annual efficiency of the export of organic carbon produced in the surface
704 layer, and its transfer to deep layers in the three study regions. We calculated the efficiency of
705 organic carbon export as the ratio of the net export at 150 m to the depth-integrated NPP. The
706 efficiency of organic carbon transfer to deep waters was defined as the ratio of net export at 800
707 m to net export at 150 m.

708 Since the modeled annual NPP showed no significant differences between the three regions
709 (Section 4.3), the overall efficiency of organic carbon export followed the same trend as exports
710 at 150 m: it was higher in deep mixing regions (Table 1). Furthermore, a similar spatial pattern
711 was found for the ratio of the net export of organic carbon at 800 m to the depth-integrated NPP.
712 No clear trend was found for the fraction of organic carbon exported below 150 m that was also
713 exported below 800 m; the only notable observation was that the highest value was found in the
714 Stratified region.

715 Henson et al. [2012] estimated that the large-scale efficiency of organic carbon transfer to the
716 deep ocean is opposite to the export efficiency; specifically, export efficiency is high (and
717 transfer efficiency low) at high latitudes, while the opposite is found at low latitudes. The authors
718 suggest that spatial variability in transfer efficiency can be explained by the structure of the

719 ecosystem. At high latitudes a diatom-dominated ecosystem favors export efficiency; material
720 that is exported below the euphotic is labile and substantially degraded in the mesopelagic zone,
721 leading to a poor deep transfer efficiency. At low latitudes, due to extensive recycling in the
722 euphotic layer, more refractory organic matter is exported under the euphotic layer, favoring
723 deep transfer efficiency. In our simulation, in the Stratified region, export at 150 m was
724 dominated by the sedimentation of large organic particles (78%), a large proportion of which
725 eventually reached deep waters. In convection regions, organic carbon was mainly exported by
726 vertical motion, meaning that it was mostly composed of small particles (heavy particles
727 represented 27% of the POC export at 150 m in the Deep Convection region). Higher transfer
728 efficiency in the Deep Convection region compared to the Shallow Convection region could then
729 be explained by the deeper mixed layer. On the one hand, intensified vertical mechanical mixing
730 supported deep transfer. On the other hand, in the Shallow Convection region, a fraction of small
731 particles that were exported at intermediate depths were remineralized before reaching 800 m, as
732 Henson et al. [2012] suggest for low latitude regions.

733 Our analysis of the DOC and POC contribution to the export at 150 and 800 m depths showed
734 that the POC export dominated total organic carbon export in the three regions (Fig. 7, Table 1).
735 Our estimation of the DOC contribution to total export in convection regions (28.7% in the Deep
736 Convection region, 22.5% in the Shallow Convection region) is close to the estimate of 20% by
737 Hansell and Carlson [1998] for the global ocean. The DOC net flux at 150 m increased the
738 efficiency of organic carbon export in convective regions (by more than 25%), while its
739 contribution was negative (−30%) in the Stratified region. The increasing contribution of DOC to
740 total export in stronger mixing regions was consistent with the fact that DOC was only exported
741 towards the bottom by turbulent mixing and vertical advection in the model, while POC was also
742 exported by sedimentation. The export of POC by sedimentation occurred throughout the year.
743 Ulses et al. [2016] used the same coupled model in the northwestern Mediterranean deep

744 convection region, and found the contribution of sedimentation export to total export ranged
 745 from 20 to 34%, with a maximum linked to the spring bloom in April/ May. In contrast, we
 746 found that DOC export under the euphotic layer was very low outside the winter mixing period,
 747 and in downwelling zones (continental slope, meso-scale vortices). As a consequence, DOC
 748 accumulated in the surface layer during the stratified period, as observed by Avril [2002] and
 749 modeled by Guyennon et al. [2016].

750 Consistent with the study of Giering et al. [2017] and Dall’Olmo et al. [2016], our results suggest
 751 that regions characterized by a clear deepening of the mixed layer may be characterized by a
 752 high export of organic carbon towards deep waters. The supply of organic carbon under the
 753 photic zone could constitute an important food source for organisms that inhabit the mesopelagic
 754 zone.

755 **Table 1:** Annual organic carbon export ($\text{gC m}^{-2} \text{ year}^{-1}$), and export and transfer efficiency in %
 756 from September 2012 to September 2013 at 150 and 800 m depths. The max (800 m, MLD)
 757 export reflects the export at depths corresponding to the maximum between 800 m and the local,
 758 annual maximum MLD.

	Deep convection	Shallow convection	Stratified
NPP 0–150m	174	190	206
POC export at 150 m	24.8	15.4	8.1
DOC export at 150 m	10.0	4.5	-1.1
POC export at 800 m	7.8	4.2	3.4
DOC export at 800 m	5.4	1.5	-1.7
POC export at max (800 m, MLD)	1.4	4.2	3.4
DOC export at max (800 m, MLD)	0.1	1.5	-1.7

POC export 150m / NPP	14.3	8.1	3.9
POC export 800m / NPP	4.5	2.2	1.6
POC export max (800m, MLD) / NPP	0.8	2.2	1.6
OC 150 m / NPP	20.0	12.4	3.0
OC 800 m / NPP	7.6	3.0	0.8
OC max (800 m, MLD) / NPP	0.9	3.0	0.8
POC export 800m / POC export 150m	31.6	27.1	41.8
POC export max (800m, MLD) / POC export 150m	5.6	27.1	41.8
OC export 800m / OC export 150 m	38.1	28.7	23.6
OC export max (800m, MLD) / OC export 150 m	4.3	28.7	23.6

759

760

5.4 Potential implications on carbon sequestration

761 The role of convection regions in terms of carbon sequestration efficiency is unclear, due to the
762 counteracting effects of convective mixing. These effects are characterized by, on the one hand,
763 an increased export of organic carbon under the euphotic layer and, on the other hand, the supply
764 in the surface layer of dissolved inorganic carbon, which is produced in deep layers by
765 remineralization of exported organic carbon. The latter effect was suggested by Copin-Montégut
766 and Bégovic [2002], who reported high values of CO₂ fugacity, and episodes of over-saturation
767 of CO₂ with respect to atmospheric equilibrium during winter wind gusts at the DYFAMED deep
768 station (Fig. 1). Our coupled simulation does not represent the dynamics of dissolved inorganic
769 carbon, and therefore only shows the initial effect of increasing OC export. According to
770 Körtzinger et al. [2008] in the North Atlantic, the physical supply of dissolved inorganic carbon
771 could have a significant effect on carbon drawdown: between 40–45% of the organic carbon

772 produced during the stratified period could be respired and reinjected into the surface layer
773 during winter mixing. Pavelsky et al. [2017] estimated this physical supply to be 40% and 90%
774 of exported organic carbon at two sites in the North Pacific. By including this mixing-induced
775 carbon supply in their budget, Pavelsky et al. [2017] found that carbon sequestration efficiency
776 was lower in regions where the mixed layer was deeper.

777 The results of our model show that if calculated below the mixed layer, deep transfer (export at
778 depths corresponding to the maximum between 800 m and the local annual maximum MLD, see
779 Section 2.3) and its efficiency were poorer in the Deep Convection region than in the two other
780 regions, in 2012/ 2013 (Table 1). Indeed, in the Deep Convection region, deep transfer was much
781 lower below the MLD than at 800 m (5 and 45 times for POC and DOC, respectively).
782 Efficiency of deep export and transfer under the annual maximum MLD falls to 11 and 17%
783 respectively compared to the flux below 800 m. In an area corresponding to one sixth of the
784 region surface, the mixed layer reached the seabed, and OC export only corresponded to the
785 deposition of POC. Moreover, the proportion of POC and DOC exported below the MLD during
786 the main convection event falls to 17 and 5% (vs. 50 and 66% at 800 m), respectively. We are
787 also showing weaker POC and DOC exports in the deep convection region compared to the other
788 regions if we interpret the result at the base of the annual maximum (800 m, MLD) rather than an
789 estimation below 150m or 800m.

790 However, two key characteristics of the hydrodynamics in this area suggest that this latter
791 assessment underestimates the amount of carbon exported under the euphotic layer and isolated
792 from the atmosphere on a decadal timescale. First, the depth of the mixed layer and the extension
793 of the convection zone show a high interannual variability in this region [*Houpert et al.*, 2016]
794 (for instance, they reported that the area of low surface chlorophyll ($<0.25 \text{ mg m}^{-3}$), considered
795 as a proxy of the deep convection zone, ranged between 1.5 and 56.3 km² between 2007/ 2008

796 and 2012/ 2013). Notably, according to Somot et al. [2016], the year 2012/ 2013 was one of the
797 strongest convective years in the period 1980–2013. Conversely, convection was probably low in
798 2013/ 2014 (owing to the especially low heat losses in ECMWF fields), suggesting that most of
799 the material exported below 800 m in 2012/ 2013 would not have been transferred back in the
800 surface (at least in 2014), and indicating an additional vertical deep transfer through POC
801 sedimentation. Second, the results of our model show a loss of organic carbon in the intermediate
802 (150–800 m) and deep layers (800 m–seabed) by lateral transport during and after convection
803 periods (an amount corresponding to 20 and 45% of the OC exported during convective periods
804 was laterally exported from the Deep Convection area into intermediate and deep layers,
805 respectively, between February and May 2013). Concomitant with this loss in the Deep
806 Convection region, a gain of OC in the Stratified region suggests that the OC that is transferred
807 to deep waters by convective events in the northern region could be transported to the southern
808 region. This is consistent with the results of Ulses et al. [2016] who calculated a north-south
809 transfer corresponding to 53% of the OC exported below 100 m, based on the same coupled
810 model. Moreover, this north–south transfer of OC in deep waters was suggested by Zúñiga et al.
811 [2007] who reported higher POC fluxes at 2145 m than at 1440 m, based on sediment trap
812 measurements. Our results are also consistent with the study of Schroeder et al. [2016] who
813 demonstrated that deep dense waters formed during convective events in the northwestern region
814 propagate throughout the western Mediterranean Sea and towards the Atlantic Ocean. It is likely
815 that these deep waters contain carbon that was exported during convection episode, which then
816 escapes from a transfer back to the surface layer in the following convective winters.

817 Finally, these findings suggest that multi-annual simulations that include the dynamics of
818 dissolved inorganic carbon are necessary to more accurately estimate the impact of convection
819 processes on the uptake of atmospheric CO₂, and to compare the net efficiency of the three
820 studied regions regarding this uptake.

821 **6. Conclusion**

822 A 3D high-resolution coupled hydrodynamic-biogeochemical model was used to study
823 phytoplankton dynamics and biogeochemical and physical carbon fluxes in three distinct regions
824 of the western Mediterranean Sea. These three regions were characterized by deep convection,
825 shallow convection, and shallow mixing during winter. Comparisons of the results of the model
826 with ocean color satellite observations presented here, and with *in situ* data presented in Kessouri
827 et al. [2017], showed that the model correctly represented the evolution over time of chlorophyll
828 in the three investigated regions.

829 The model confirms that regimes similar to subpolar and subtropical regimes coexist in the
830 western Mediterranean Sea, within a distance of several hundreds of kilometers, in response to
831 contrasting winter mixing conditions (Fig. 9). Although this has already been established from
832 the annual surface chlorophyll cycle, here we confirm it, based on a broader description of the
833 functioning of the planktonic ecosystem.

834 The conditions of bloom onset do not significantly differ from those already described in other
835 regions. However, in the case of the autumn bloom, we found that an increase in surface
836 chlorophyll did not correspond to bloom onset, but rather to the erosion of the DCM. In the case
837 of the specific period studied here, the “real” bloom (corresponding to an increase in integrated
838 biomass) occurred one month later, when the mixed layer reached the nutricline. The winter/
839 early spring bloom, as it is known in the North Atlantic, was only identified in the Deep
840 Convection region. The processes triggering this bloom correspond to earlier descriptions of
841 subpolar regions, with the first condition being the breakdown of turbulence. In the northwestern
842 convection region, we identified the importance of restratification, due to baroclinic instabilities
843 that developed rapidly after the change in sign of surface heat fluxes. This process thinned the

844 mixed layer. This indicates that the difference between the active mixed layer (corresponding to
845 a period of surface heat losses) and the passive mixed layer (after the change in sign of heat
846 fluxes) is not relevant in explaining the breakdown of turbulence. This is at least true at the
847 periphery of the convective zone, which was rapidly affected by frontal instabilities. As
848 expected, the low grazing pressure brought about by convection through dilution allowed the
849 explosion of the bloom.

850 NPP differences between the stratified and convective regions were considered insignificant
851 because of opposing biases in the simulated surface chlorophyll in these regions. In deep
852 convection regions, the inhibition of winter productivity during the two-month period of the deep
853 mixed layer contributed to reduce primary production. In contrast to annual primary production,
854 annual export of organic carbon and its deep transfer were very different in convective and
855 stratified regions in 2012/ 2013. Deep convection produced an export of particulate organic
856 matter that was 3.5 (2.3) times higher than in the stratified region below 150 (800) m, while for
857 total (particulate + dissolved) organic carbon, this ratio reached 5.0 (8.0) below 150 (800) m. The
858 consequence of the two points described above is that export efficiency (export/ primary
859 production) was much higher in convective regions than in the stratified region. This is largely
860 the result of the mixed layer pump process described by Dall’Olmo et al. [2016], which
861 transports POC and DOC to great depths. The results of the model showed that in the deep
862 convection region, export at 150 m during the convection period represented 60% (70%) of the
863 annual export of POC (DOC). These results suggest that the higher amount of organic matter
864 transferred to deep waters, and representing a food source for marine organisms, may make the
865 northwestern Mediterranean convection areas a favorable habitat for the mesopelagic ecosystem.
866 Furthermore, they highlight the importance of monitoring convective regions, as they may be
867 modified in response to climate warming, supporting the development of a regime similar to the

868 subtropical regime with a lower deep transfer rate. Our estimation of the POC and DOC exports
869 as well as their transfer and efficiency rates below the annual maximum (MLD, 800 m) are lower
870 in the deep convection region compared to the two other regions. These low rates are due to the
871 lateral transfer of the exported matter from the deep convection region to the adjacent regions.

872 Our analysis, which relied mainly on vertical mixing, did not investigate the coupling between
873 different regions of the Mediterranean that, in the long term, governs the spatial distribution of
874 nutrients. Thermohaline circulation produces a rather complex circulation of the different water
875 masses. In the context of the present paper, Atlantic waters flow into the Algerian sub-basin, and
876 a part of them reaches then the Gulf of Lions convection zone taking a cyclonic path through the
877 western basin. The deep waters formed in the Gulf of Lions are dispersed towards the Algerian
878 sub-basin and feed the deep waters of the western basin. Finally, the Levantine intermediate
879 waters link the eastern and western basins. Formed in the Rhodes gyre in the Levantine basin,
880 they collect organic matter sinking from the surface, which is recycled into nutrients [*Crise et al.*,
881 1999], part of which is ultimately exported to the Atlantic. During convection in the Gulf of
882 Lions, the nutrients transported in intermediate waters are mixed over the water column and fuel
883 the nutrient pool of surface and deep waters. We have seen that convection exports organic
884 matter. A consequence of deep circulation is horizontal transport of this organic matter towards
885 the Algerian basin. In this context, we refer to the quantification of Ulses et al. [2016], who
886 found the transfer to the Algerian sub-basin deep waters (100 m–seabed) was equivalent to 53%
887 of the OC exported below 100 m in the convective region ($337 \cdot 10^4 \text{ tC y}^{-1}$). An additional $165 \cdot 10^4$
888 tC y^{-1} was conveyed in the first 100 m. These advective processes are thought to create a
889 coupling between the three regions, and their consequences, notably on carbon sequestration
890 deserve more attention.

891 To conclude, it is worth restating that the results presented in the present study relate to one year,

892 characterized by strong convection in the northwestern Mediterranean. This is supported by the
893 work of Somot et al. [2016] (from a model), Mayot et al. [2017b] (from satellite chlorophyll),
894 and Herrmann et al. [2017] (from an analysis of altimetry and surface chlorophyll). These results
895 should be revisited on an interannual basis, when convection is variable. Ulses et al. [2016]
896 found that during mild winters, surface chlorophyll in the deep convection area increases almost
897 constantly from January to mid-March. The authors also found low interannual variability in
898 primary production (~ 4%), and a POC and DOC export at 100 m of about two times higher for
899 years with strong convection than with weak convection. The differences found in our study
900 between the Deep Convection region and the two other regions are generally consistent with
901 these results, and support the argument that the depth of the mixed layer plays a major role in the
902 control of phytoplankton dynamics.

903 **Acknowledgements**

904 This study has been funded by the PERSEUS project (European Union FP7 Grant Agreement
905 287600). It is a contribution to the MerMex (Marine Ecosystem Response in the Mediterranean
906 Experiment) project of the MISTRALS international program. Numerical simulations were
907 performed using the computing cluster of Laboratoire d'Aérodologie and HPC resources from
908 CALMIP (grants P1325, P09115 and P1331). We thank two anonymous reviewers for
909 constructive comments. We thank NASA for providing surface chlorophyll data
910 (10.5067/NIMBUS-7/CZCS/L3B/CHL/2014).

911

912 **Table caption**

913 **Table 1:** Annual organic carbon export ($\text{gC m}^{-2} \text{ year}^{-1}$), and export and transfer efficiency in %
914 from September 2012 to September 2013 at 150 and 800 m depths. The max (800 m, MLD)
915 export reflects the export at depths corresponding to the maximum between 800 m and the local,
916 annual maximum MLD.

917 **Figure captions**

918 **Figure 1.** Location of the modeled area in the Western Mediterranean Sea. The colored regions
919 correspond to the three regions considered in this study: the Deep Convection area (DCA, red),
920 Shallow Convection area (SCA, blue) and Stratified area (STA, green).

921 **Figure 2.** (Upper panel) Taylor diagram comparing the simulated and observed surface
922 chlorophyll concentrations, where OBS indicates MODIS data and DCA, SCA and STA indicate
923 the model outputs in the Deep Convection region, Shallow Convection region, and Stratified

924 region, respectively. (Lower panel) Time series of the simulated (black line, median; gray bar,
925 standard deviation) and observed (colored points and colored blue bars for standard deviation)
926 surface chlorophyll concentrations (in mg m^{-3}) in three western Mediterranean regions: the Deep
927 Convection region (DCA, red points), Shallow Convection region (SCA, blue points) and
928 Stratified region (STA, green points) from September 2012 to September 2013. The vertical
929 dashed lines represent the dates of the blooms onset (see Section 5.1 and Fig. 6).

930 **Figure 3.** Comparison between the simulated and MODIS chlorophyll concentration (mg m^{-3}) in
931 winter (19 February 2013, A and B) and spring (14 April 2013, C and D).

932 **Figure 4.** Time series of the spatially averaged heat flux (W m^{-2}) calculated for the three studied
933 regions: Deep Convection area in red, Shallow Convection area in blue and stratified area in
934 green. The dates of the blooms onsets are indicated with arrows (see Section 5.1).

935 **Figure 5.** Top panel represents the temporal evolution of the simulated MLD (m) in the Deep
936 Convection region (black), the Shallow Convection region (blue) and the Stratified region
937 (green) from September 2012 to September 2013. The y-axis is logarithmic. The other panels
938 represent the chlorophyll concentration (mg m^{-3}) averaged in each of the studied regions (Deep
939 Convection region, Shallow Convection region and Stratified region, from upper to lower panel,
940 respectively). The MLD is superimposed (white line). Arrows indicate the bloom onsets (see
941 Section 5.1).

942 **Figure 6.** Time series from September 2012 to September 2013 of the simulated net primary
943 production (NPP) ($\text{gC m}^{-2} \text{ day}^{-1}$) spatially averaged (red) and standard deviation (grey) in the
944 Deep Convection (DCA, left), Shallow Convection (SCA, middle) and Stratified (STA, right)
945 regions. Vertical arrows indicate the blooms onset (See Section 5.1).

946 **Figure 7.** Time series from September 2012 to September 2013 of the modeled particulate
947 (upper panel) and dissolved (lower panel) organic carbon export ($\text{mgC m}^{-2} \text{ day}^{-1}$) at 150 m depth
948 in red and 800m in blue, in the Deep Convection Area (DCA, left), Shallow Convection Area
949 (SCA, middle) and Stratified Area (STA, right). The first blue bar corresponds to the main
950 convection event and the second blue bar represents the short deep mixing event of the third
951 week of March.

952 **Figure 8.** Time series from September 2012 to September 2013 of (a, g, m) modeled depth-
953 integrated phytoplankton biomass (mgC m^{-2}) in red and surface chlorophyll concentration (mmol
954 m^{-3}) in black, (b, h, n) net heat flux (W m^{-2}) with heat losses in blue and heat gains in red, (c, i, o)
955 MLD (m), (d, j, p) the 0-75 m averaged turbulent diffusivity ($\text{m}^2 \text{ s}^{-1}$), (e, k, q) depth-integrated
956 zooplankton biomass in black (mgC m^{-2}) and grazing rate in red ($\text{mgC m}^{-2} \text{ day}^{-1}$), and (f, l, r)
957 nitrate (in black) and phosphate (in red) surface concentrations (mmol.m^{-3}), in the Deep
958 Convection area (DCA, left), the Shallow Convection area (SCA, middle) and the Stratified area
959 (STA, right). Vertical dashed lines indicate the dates of the bloom onsets (black=using surface
960 chlorophyll, red=using the vertically integrated biomass).

961 **Figure 9.** Conceptual model representing plankton and particles behavior for three different
962 regimes in the western Mediterranean Sea. This conceptual model resumes the various sequences
963 from the destruction of the DCM, the injection of nutrients to the euphotic layer, the deep mixing
964 of the living cells (in the 1st region), the triggering of the blooms and the new setting up of the
965 DCM affected by different strength mixing. These sequences are shown simultaneously with
966 different ways of small and large organic particles export and trapping below the euphotic layer
967 via the mixing layer pump.

968

969 **References**

970 Allen, J. I., P. J. Somerfield, and J. Siddorn (2002), Primary and bacterial production in the
971 Mediterranean Sea: A modelling study, *J. Mar. Syst.*, 33-34, 473–495, doi:10.1016/S0924-
972 7963(02)00072-6.

973 Anderson, T. R., and P. Pondaven (2003), Non-redfield carbon and nitrogen cycling in the Sargasso
974 Sea: Pelagic imbalances and export flux, *Deep Sea Res., Part I*, 50, 573–591.

975 Auger, P. A., F. Diaz, C. Ulses, C. Estournel, J. Neveux, F. Joux, M. Pujo-Pay, and J.J. Naudin
976 (2011), Functioning of the planktonic ecosystem on the Gulf of Lions shelf (NW
977 Mediterranean) during spring and its impact on the carbon deposition: A field data and 3-D
978 modelling combined approach, *Biogeosciences*, 8(11), 3231–3261, doi:10.5194/bg-8-3231-
979 2011.

980 Auger, P. A., C. Ulses, C. Estournel, L. Stemmann, S. Somot, and F. Diaz (2014), Interannual
981 control of plankton communities by deep winter mixing and prey/predator interactions in the
982 NW Mediterranean: Results from a 30-year 3D modeling study, *Prog. Oceanogr.*, 124, 12–
983 27, doi:10.1016/j.pocean.2014.04.004.

984 Avril, B. (2002), DOC dynamics in the Northwestern Mediterranean Sea (DyFaMed site), *Deep-Sea*
985 *Res. II*, 49, 2163–2182.

986 Baklouti, M., V. Faure, L. Pawlowski, and A. Sciandra (2006), Investigation and sensitivity analysis
987 of a mechanistic phytoplankton model implemented in a new modular *numerical tool*
988 (*Eco3M*) dedicated to biogeochemical modelling, *Prog. Oceanogr.*, 71(1), 34–58,
989 doi:10.1016/j.pocean.2006.05.003.

- 990 Behrenfeld, M.J. (2010), Abandoning Sverdrup's critical depth hypothesis on phytoplankton
991 blooms. *Ecology*, 91: 977–989.
- 992 Behrenfeld, M.J. and E.S. Boss (2014), Resurrecting the ecological underpinnings of ocean plankton
993 blooms. *Annu. Rev. Mar. Sci.*, 6:167–94.
- 994 Ben Rais Lasram, F., F. Guilhaumon, C.Albouy, S. Somot, W. Thuillier, and D. Mouillot (2010),
995 The Mediterranean Sea as a 'cul-de-sac' for endemic fishes facing climate change. *Global*
996 *Change Biology*, 16: 3233–3245. doi:10.1111/j.1365-2486.2010.02224.x
- 997 Bentsen, M., G. Evensen , H. Drange, and A.D. Jenkins (1999), Coordinate Transformation on a
998 Sphere Using Conformal Mapping, *Mon. Wea. Rev.*, 127, 2733-2740
- 999 Bernardello, R., J. G. Cardoso, N. Bahamon, D. Donis, I. Marinov,. and A. Cruzado (2012), Factors
1000 controlling interannual variability of vertical organic matter export and phytoplankton bloom
1001 dynamics-a numerical case-study for the NW Mediterranean Sea, *Biogeosciences*, 9, 4233-
1002 4245, doi:10.5194/bg-9-4233-2012.
- 1003 Bethoux J.P, (1989), Oxygen consumption, new production, vertical advection and environmental
1004 evolution in the Mediterranean Sea. *Deep Sea Research Part A. Oceanographic Research*
1005 *Papers*. Volume 36, Issue 5, May 1989, Pages 769-781. [https://doi.org/10.1016/0198-](https://doi.org/10.1016/0198-0149(89)90150-7)
1006 [0149\(89\)90150-7](https://doi.org/10.1016/0198-0149(89)90150-7)
- 1007 Bishop, J. K. B., M. H. Conte., P. H. Wiebe, M. R.Roman and C. Langdon (1986), Particulate
1008 matter production and consumption in deep mixed layers—observations in a warm-core ring.
1009 *Deep-Sea Res. A*, 33, 1813–1841.
- 1010 Bosc, E., A.. Bricaud, and D. Antoine (2004), Seasonal and interannual variability in algal biomass

- 1011 and primary production in the Mediterranean Sea, as derived from 4 years of SeaWiFS
1012 observations, *Global Biogeochem. Cycles*, 18(1), 1–17, doi:10.1029/2003GB002034.
- 1013 Brody, S. R., M. S. Lozier, and J. P. Dunne (2013), A comparison of methods to determine
1014 phytoplankton bloom initiation, *J. Geophys. Res. Oceans*, 118, 2345–2357,
1015 doi:10.1002/jgrc.20167.
- 1016 Brody, S. R., and M. S. Lozier. (2015), Characterizing upper-ocean mixing and its effect on the
1017 spring phytoplankton bloom with in situ data. *ICES Journal of Marine Science*;
1018 doi:10.1093/icesjms/fsv006
- 1019 Buesseler, K. O., (2007), An assessment of the use of sediment traps for estimating upper ocean
1020 particle fluxes. *Journal of Marine Research*, 65, 345–416, 2007
- 1021 Chiswell, S. M., J. Bradford-Grieve, M. G. Hadfield, and S. C. Kennan (2013), Climatology of
1022 surface chlorophyll a, autumn-winter and spring blooms in the southwest Pacific Ocean, *J.*
1023 *Geophys. Res. Oceans* , 118, 1003–1018, doi:10.1002/jgrc.20088.
- 1024 Copin-Montégut, G., and B. Avril (1993), Vertical distribution and temporal variation of dissolved
1025 organic carbon in the North-Western Mediterranean Sea, *Deep-Sea Res. I*, 40(10), 1963-
1026 1972.
- 1027 Copin-Montégut, C. and M. Bégovic (2002), Distributions of carbonate properties and oxygen along
1028 the water column (0–2000 m) in the central part of the NW Mediterranean Sea (Dyfamed
1029 site): influence of winter vertical mixing on air–sea CO₂ and O₂ exchanges. *Deep Sea*
1030 *Research Part II: Topical Studies in Oceanography*, 49, 11, 2049–2066. doi:[10.1016/S0967-](https://doi.org/10.1016/S0967-0645(02)00027-9)
1031 [0645\(02\)00027-9](https://doi.org/10.1016/S0967-0645(02)00027-9)

- 1032 Coppola, L., L. Prieur, I. Taupier-Letage, C. Estournel, P. Testor, D. Lefevre, S. Belamari, S.
1033 LeReste, and V. Taillandier (2017), Observation of oxygen ventilation into deep waters
1034 through targeted deployment of multiple Argo-O₂ floats in the north-western Mediterranean
1035 Sea in 2013, *J. Geophys. Res. Oceans*, 122, 6325–6341, doi:10.1002/2016JC012594.
- 1036 Crise, A., J. I Allen, J. Baretta , G. Crispi, R. Mosetti, C. Solidoro (1999), The Mediterranean
1037 pelagic ecosystem to physical forcing. *Progress in Oceanography*, 44 (1999) 219–243.
- 1038 Crispi, G., A. Crise, and C. Solidoro (2002), Coupled Mediterranean ecomodel of the phosphorus
1039 and nitrogen cycles. *Journal of Marine Systems* 33– 34 p497– 521.
- 1040 Dall’Olmo, G. J., Dingle, L. Polimene, R. J. W. Brewinn and H. Claustre (2016), Substantial energy
1041 input to the mesopelagic ecosystem from the seasonal mixed-layer pump. *Nature*
1042 *Geoscience*, 9, 820–823, doi:10.1038/ngeo2818
- 1043 D’Ortenzio, F., and M. Ribera d’Alcalà (2009), On the trophic regimes of the Mediterranean Sea: a
1044 satellite analysis, *Biogeosciences*, 6, 139-148, doi:10.5194/bg-6-139-2009.
- 1045 D’Ortenzio, F., H. Lavigne, F. Besson, H. Claustre, L. Coppola, N. Garcia, A. Laës-Huon, S. Le
1046 Reste, D. Malardé, C. Migon, P. Morin, L. Mortier, A. Poteau, L. Prieur, P. Raimbault, and
1047 P. Testor (2014), Observing mixed layer depth, nitrate and chlorophyll concentrations in the
1048 northwestern Mediterranean: A combined satellite and NO₃ profiling floats experiment,
1049 *Geophys. Res. Lett.*, 41, 6443–6451, doi:[10.1002/2014GL061020](https://doi.org/10.1002/2014GL061020).
- 1050 Durrieu de Madron, X. and Mermex Group (2011), Marine ecosystems’ responses to climatic and
1051 anthropogenic forcings in the Mediterranean. *Prog. Oceanogr.*, 91(2), 97–166.
1052 doi:10.1016/j.pocean.2011.02.003.

1053 Estournel C., P. Testor, I. Taupier-Letage, M.N. Bouin, L. Coppola, P. Durand, P. Conan, A.
1054 Bosse, P.E. Brilouet, L. Beguery, S. Belamari, K. Béranger, J. Beuvier, D. Bourras, G.
1055 Canut, A. Doerenbecher, X. Durrieu de Madron, F. D'Ortenzio, P. Drobinski, V. Ducrocq, N.
1056 Fourrié, H. Giordani, L. Houpert, L. Labatut, C. Lebeau-pin Brossier, M. Nuret, L. Prieur, O.
1057 Roussot, L. Seyfried, and S. Somot (2016a), HyMeX-SOP2, the field campaign dedicated to
1058 dense water formation in the north-western Mediterranean, *Oceanography*, 29,4.

1059 Estournel C., P. Testor, P. Damien, F. D'Ortenzio, P. Marsaleix, P. Conan, F. Kessouri, X.
1060 Durrieu de Madron, L. Coppola, J.M. Lellouche, S. Belamari, L. Mortier, C. Ulses, M.N.
1061 Bouin, and L. Prieur (2016b), High resolution modeling of dense water formation in the
1062 north-western Mediterranean during winter 2012-2013: Processes and budget, *J. Geophys.*
1063 *Res. Oceans*, 121, 5367–5392, doi:[10.1002/2016JC011935](https://doi.org/10.1002/2016JC011935).

1064 Gardner, W. D., S. P. Chung, M. J. Richardson, and I. D. Walsh (1995), The oceanic mixed-layer
1065 pump. *Deep-Sea Res. II*, 42, 757–775.

1066 Giering, S. L. C., R. Sanders, A. P. Martin, S. A. Henson, J. S. Riley, C. M. Marsay, and D. G.
1067 Johns (2017), Particle flux in the oceans: Challenging the steady state assumption, *Global*
1068 *Biogeochem. Cycles*, 31, 159–171, doi:[10.1002/2016GB005424](https://doi.org/10.1002/2016GB005424).

1069 Gogou, A., A. Sanchez-Vidal, X. Durrieu de Madron, S. Stavrakakis, A.M. Calafat, M. Stabholz, S.
1070 Psarra, M. Canals, S. Heussner, I. Stavrakaki, and E. Papathanassiou (2014), Carbon flux
1071 to the deep in three open sites of the Southern European Seas (SES), *J. Mar. Syst.*, 135, 170–
1072 179, doi:[10.1016/j.jmarsys.2014.04.012](https://doi.org/10.1016/j.jmarsys.2014.04.012).

1073 Guyennon, A., M. Baklouti, F. Diaz, J. Palmieri, J. Beuvier, C. Lebeau-pin-Brossier, T. Arsouze, K.
1074 Béranger, J.-C. Dutay, and T. Moutin (2015), New insights into the organic carbon export in

- 1075 the Mediterranean Sea from 3-D modeling, *Biogeosciences*, 12, 7025-7046, doi:10.5194/bg-
1076 12-7025-2015, 2015.
- 1077 Hansell, D. A., and C. A. Carlson (1998), Net community production of dissolved organic carbon,
1078 *Global Biogeochem. Cycles*, 12(3), 443–453, doi:10.1029/98GB01928.
- 1079 Helbling E. W. and V. E. Villafane (2009), *Phytoplankton and Primary Production in Fisheries and*
1080 *Aquaculture - Volume 5*. No. of Pages:458. ISBN:978-1-84826-112-9 (eBook), ISBN: 978-
1081 1-84826-562-2 (Print Volume).
- 1082 Henson, S., J. Dunne, and J. Sarmiento (2009), Decadal variability in North Atlantic phytoplankton
1083 blooms. *J. Geophys. Res.*, 114, C04013, doi:[10.1029/2008JC005139](https://doi.org/10.1029/2008JC005139).
- 1084 Henson, S. A., R. Sanders, and E. Madsen (2012), Global patterns in efficiency of particulate
1085 organic carbon export and transfer to the deep ocean, *Global Biogeochem. Cycles*, 26,
1086 GB1028, doi:[10.1029/2011GB004099](https://doi.org/10.1029/2011GB004099).
- 1087 Herrmann, M., F. Diaz, C. Estournel, P. Marsaleix and C. Ulses (2013), Impact of atmospheric and
1088 oceanic interannual variability on the Northwestern Mediterranean Sea pelagic planktonic
1089 ecosystem and associated carbon cycle, *J. Geophys. Res. Oceans*, 118, 5792–5813,
1090 doi:[10.1002/jgrc.20405](https://doi.org/10.1002/jgrc.20405).
- 1091 Herrmann, M., P.-A. Auger, C. Ulses, and C. Estournel (2017), Long-term monitoring of ocean
1092 deep convection using multisensors altimetry and ocean color satellite data, *J. Geophys. Res.*
1093 *Oceans*, 122, 1457–1475, doi:[10.1002/2016JC011833](https://doi.org/10.1002/2016JC011833).
- 1094 Ho, C. and J. Marra, (1994) Early-spring export of phytoplankton production in the northeast
1095 Atlantic-ocean. *Mar. Ecol. Prog. Ser.* 114, 197–202.
- 1096 Houpert, L., P. Testor, X. Durrieu de Madron, S. Somot, F. D'Ortenzio, C. Estournel and H.

- 1097 Lavigne (2015). Seasonal cycle of the mixed layer, the seasonal thermocline and the upper-
1098 ocean heat storage rate in the Mediterranean Sea derived from observations. *Progress in*
1099 *Oceanography*, 132, 333-352
- 1100 Houpert, L., X. Durrieu de Madron, P. Testor, A. Bosse, F. D'Ortenzio, et al. (2016). Observations
1101 of open-ocean deep convection in the northwestern Mediterranean Sea: Seasonal and
1102 interannual variability of mixing and deep water masses for the 2007-2013 Period. *Journal*
1103 *of Geophysical Research. Oceans*, 121, pp.8139-8171 <[10.1002/2016JC011857](https://doi.org/10.1002/2016JC011857)>.
- 1104 Kessouri, F., C. Ulses, C. Estournel, P. Marsaleix, T. Severin, M. Pujo-Pay, J. Caparros, P.
1105 Raimbault, O. Pasqueron de Fommervault, F. D'Ortenzio, V. Taillandier, P. Testor, P.
1106 Conan. Nitrogen and phosphorus budgets in the Northwestern Mediterranean deep
1107 convection region. (2017). DOI: [10.1002/2016JC012665](https://doi.org/10.1002/2016JC012665) *Journal of Geophysical Research*
1108 *Oceans*.
- 1109 Klein B., Roether W., Manca B.B., Bregant D., Beitzel V., Kovacevic V., and A. Luchetta, (1999)
1110 The large deep water transient in the Eastern Mediterranean, *Deep Sea Research Part I*, 46,
1111 3, 371-414
- 1112 Koeve, W. (2001), Wintertime nutrients in the North Atlantic—New approaches and implications
1113 for new production estimates. *Mar. Chem.*, 74, 245–260.
- 1114 Körtzinger, A. U. Send, R. S. Lampitt, S. Hartman, D. W. R. Wallace, J. Karstensen, M. G.
1115 Villagarcia, O. Llina, and M. D. DeGrandpre (2008), The seasonal pCO₂ cycle at 49 degrees
1116 N/16.5 degrees W in the northeastern Atlantic Ocean and what it tells us about biological
1117 productivity. *J. Geophys. Res.*, 113, 1–15 (2008).
- 1118 Large, W. G. and S. Yeager (2009), The global climatology of an interannually varying air-sea flux

- 1119 data set. *Clim. Dyn.*, *33*, 341–364, doi:10.1007/s00382-008-0441-3.
- 1120 Lavigne, H., F. D'Ortenzio, C. Migon, H. Claustre, P. Testor, M. Ribera d'Alcalà, R. Lavezza, L.
1121 Houpert, and L. Prieur (2013), Enhancing the comprehension of mixed layer depth control
1122 on the Mediterranean phytoplankton phenology, *J. Geophys. Res. Oceans*, *118*, 3416–3430,
1123 doi:10.1002/jgrc.20251.
- 1124 Lavigne, H., F. D'Ortenzio, M. Ribera D'Alcalà, H. Claustre, R. Sauzède, and M. Gacic (2015), On
1125 the vertical distribution of the chlorophyll a concentration in the Mediterranean Sea: a basin
1126 scale and seasonal approach, *Biogeosciences*, *12*, 5021-5039, doi:10.5194/bg-12-5021-2015
- 1127 Laws, E. A., E. D'Sa, and P. Naik (2011), Simple equations to estimate ratios of new or export
1128 production to total production from satellite-derived estimates of sea surface temperature and
1129 primary production, *Limnol. Ocean. Methods*, *9*, 593–601, doi:10.4319/lom.2011.9.593.
- 1130 Lazzari, P., C. Solidoro, V. Ibello, S. Salon, A. Teruzzi, K. Béranger, S. Colella, and A. Crise
1131 (2012), Seasonal and inter-annual variability of plankton chlorophyll and primary production
1132 in the Mediterranean Sea: A modelling approach, *Biogeosciences*, *9*, 217-233,
1133 doi:10.5194/bg-9-217-2012
- 1134 Lellouche, J.-M., O. Le Galloudec, M. Drévillon, C. Régnier, E. Greiner, G. Garric, N. Ferry, C.
1135 Desportes, C.E. Testut, C. Bricaud, R. Bourdallé-Badie, B. Tranchant, M. Benkiran, Y.
1136 Drillet, A. Daudin, and C. De Nicola (2013), Evaluation of global monitoring and
1137 forecasting systems at Mercator Océan, *Ocean Sci.*, *9*, 57-81, doi:10.5194/os-9-57-2013.
- 1138 Ludwig, W., A. F. Bouwman, E. Dumont, and F. Lespinas (2010), Water and nutrient fluxes from
1139 major Mediterranean and Black Sea rivers: Past and future trends and their implications for
1140 the basin-scale budgets, *Global Biogeochem. Cycles*, *24*, GB0A13,

1141 doi:[10.1029/2009GB003594](https://doi.org/10.1029/2009GB003594).

1142 Macias, D., E. Garcia-Gorriz, C. Piroddi, and A. Stips (2014), Biogeochemical control of marine
1143 productivity in the Mediterranean Sea during the last 50 years, *Global Biogeochem. Cycles*,
1144 28, doi:[10.1002/2014GB004846](https://doi.org/10.1002/2014GB004846).

1145 Mahadevan, A., E. D'Asaro, C. Lee, M-J. Perry (2112). Eddy-Driven Stratification Initiates North
1146 Atlantic Spring Phytoplankton Blooms. *Science*, 337, 6090, 54-58, DOI:
1147 [10.1126/science.1218740](https://doi.org/10.1126/science.1218740)

1148 Manca, M., M. Burca, A. Giorgetti, C. Coatanoan, M.J. Garcia, and A. Iona (2004), Physical and
1149 biochemical averaged vertical profiles in the Mediterranean regions: an important tool to
1150 trace the climatology of water masses and to validate incoming data from operational
1151 oceanography, *J. Mar. Syst.*, 48, 1–4, 83-116.

1152 Maraldi, C., J. Chanut, B. Levier, N. Ayoub, P. De Mey, G. Reffray, F. Lyard, S. Cailleau, M.
1153 Drevillon, E.A. Fanjul, M.G. Sotillo, P. Marsaleix, and the Mercator Research and
1154 Development Team (2013), NEMO on the shelf: assessment of the Iberia–Biscay–Ireland
1155 configuration. *Ocean Sci.*, 9, 745–771. <http://dx.doi.org/10.5194/os-9-745-2013>.

1156 Marsaleix, P., F. Auclair, J. W. Floor, M. J. Herrmann, C. Estournel, I. Pairaud, and C. Ulses
1157 (2008), Energy conservation issues in sigma-coordinate free-surface ocean models, *Ocean*
1158 *Modell.*, 20, 61–89.

1159 Marsaleix, P., F. Auclair, and C. Estournel (2009), Low-order pressure gradient schemes in sigma
1160 coordinate models: The seamount test revisited, *Ocean Modell.*, 30, 169–177,
1161 doi:[10.1016/j.ocemod.2009.06.011](https://doi.org/10.1016/j.ocemod.2009.06.011).

1162 Marsaleix, P., F. Auclair, C. Estournel, C. Nguyen, and C. Ulses (2011), An accurate
1163 implementation of the compressibility terms in the equation of state in a low order pressure
1164 gradient scheme for sigma coordinate ocean models, *Ocean Modell.*, *40*, 1-13
1165 doi:10.1016/j.ocemod.2011.07.004

1166 Marsaleix, P., F. Auclair, T. Duhaut, C. Estournel, C. Nguyen, and C. Ulses (2012), Alternatives to
1167 the Robert-Asselin filter, *Ocean Modell.*, *41*, 53–66, doi:10.1016/j.ocemod.2011.11.002.

1168 Marty, J.C, and J. Chiaverini (2002). Seasonal and interannual variations in phytoplankton
1169 production at DYFAMED time-series station, northwestern Mediterranean Sea, *Deep-Sea*
1170 *Res. II*, *49(11)*, 2017-20130.

1171 Mayot, N., F. D’Ortenzio, M. Ribera d’Alcalà, H. Lavigne, and H. Claustre (2016), Interannual
1172 variability of the Mediterranean trophic regimes from ocean color satellites, *Biogeosciences*,
1173 *13*, 1901–1917

1174 Mayot, N., F. D’Ortenzio, V. Taillandier, L. Prieur, O. Pasqueron de Fommervault, H. Claustre, A.
1175 Bosse, P. Testor and P. Conan (2017a), Physical and biogeochemical controls of the
1176 phytoplankton blooms in North Western Mediterranean Sea: a multiplatform approach over
1177 a complete annual cycle (2012-2013 DEWEX experiment), In press, *Journal of Geophysical*
1178 *Research: Oceans*, doi:10.1002/2016JC012668.

1179 Mayot N., F. D’Ortenzio, J. Uitz, B. Gentili, J. Ras, V. Vellucci, M. Golbol, D. Antoine and H.
1180 Claustre (2017b) Influence of the phytoplankton community structure on the spring and
1181 annual primary production in the North-Western Mediterranean Sea. In press, *Journal of*
1182 *Geophysical Research: Oceans*, DOI: 10.1002/2016JC012668

1183 MERMEX Group, 2011. Marine ecosystems responses to climatic and anthropogenic forcings in the
1184 Mediterranean. *Prog. Oceanogr.* 91:97–166. <http://dx.doi.org/10.1016/j.pocean.2011.02.003>

1185 Miquel, J. C., J. Martín, B. Gasser, A. Rodriguez-y-Baena, T. Toubal, and S.W. Fowler (2011),
1186 Dynamics of particle flux and carbon export in the northwestern Mediterranean Sea: A two
1187 decade time-series study at the DYFAMED site, *Prog. Oceanogr.*, 91(4), 461–481,
1188 doi:10.1016/j.pocean.2011.07.018

1189 Moutin, T., P. Raimbault, H.L. Golterman, and B. Coste (1998), The input of nutrients by the Rhône
1190 river into the Mediterranean Sea: recent observations and comparison with earlier data,
1191 *Hydrobiologia*, 373: 237. doi:10.1023/A:1017020818701

1192 Pastor, L., B. Deflandre, E. Viollier, C. Cathalot, E Metzger, C. Rabouille, K. Escoubeyrou, E.
1193 Lloret, A.M. Pruski, G. Vétion, M. Desmalades, R. Buscail, and A. Grémare (2011),
1194 Influence of the organic matter composition on benthic oxygen demand in the Rhône River
1195 prodelta (NW Mediterranean Sea), *Cont. Shelf Res.*, 31(9), 1008–1019,
1196 doi:10.1016/j.csr.2011.03.007

1197 Palevsky, H. I., and P. D. Quay (2017), Influence of biological carbon export on ocean carbon
1198 uptake over the annual cycle across the North Pacific Ocean, *Global Biogeochem.*
1199 *Cycles*, 31, 81–95, doi:[10.1002/2016GB005527](https://doi.org/10.1002/2016GB005527).

1200 Petrenko, A., C. Dufau, and C. Estournel (2008), Barotropic eastward currents in the western Gulf
1201 of Lion, north-western Mediterranean Sea, during stratified conditions, *J. Mar. Syst.*, 74,
1202 406–428 doi:[10.1016/j.jmarsys.2008.03.004](https://doi.org/10.1016/j.jmarsys.2008.03.004)

1203 Roether, W., Manca, B.B., Klein, B., Bregant, D., Georgopoulos, D., Beitzel, V., Kovacevic, V.,
1204 and A. Luchetta (1996), Recent changes in Eastern Mediterranean deep waters. *Science* 271,

1205 333–335.

1206 Rubio, A., B. Barnier, G. Jorda, M. Espino, and P. Marsaleix (2009), Origin and dynamics of
1207 mesoscale eddies in the Catalan Sea (NW Mediterranean): Insight from a numerical model
1208 study, *J. Geophys. Res.*, *114*, C06009, doi:10.1029/2007JC004245

1209 Santinelli, C., L. Nannicini, and A. Seritti (2010), DOC dynamics in the meso and bathypelagic
1210 layers of the Mediterranean Sea. *Deep-Sea Res. II*, *57*, 1446–1459.

1211 Schroeder, K., Ribotti, A., Borghini, M., Sorgente, R., Perilli, A., and Gasparini, G.P.: An extensive
1212 Mediterranean deep water renewal between 2004 and 2006, (2016), *Geophysical Research*
1213 *Letters*, *35*, L18605, doi: 10.1029/2008GL035146, 2008. Schroeder, K., Chiggiato, J.,
1214 Bryden, H.L., Borghini, M., and Ben Ismail, S.: Abrupt climate shift in the Western
1215 Mediterranean Sea. *Scientific Reports*, *6*:23009, doi: 10.1038/srep23009.

1216 Sempéré, R., B. Charrière, F. Van Wambeke, and G. Cauwet (2000), Carbon Inputs of the Rhône
1217 River to the Mediterranean Sea: Biogeochemical Implications, *Global Biogeochem. Cycles*,
1218 *14*, 2, 669–681.

1219 Severin, T., Kessouri .F, Rembauville, M., et al. (2017), Open-ocean convection process: A driver
1220 of the winter nutrient supply and the spring phytoplankton distribution in the Northwestern
1221 Mediterranean Sea, *J. Geophys. Res. Oceans*, *122*, doi:10.1002/2016JC012664.

1222 Siegel, D.A., S.C. Doney, and J.A. Yoder (2002), The North Atlantic spring phytoplankton bloom
1223 and Sverdrup's critical depth hypothesis, *Science*, *296*, 730–733, DOI:
1224 10.1126/science.1069174

- 1225 Siegel, D. A., K. O. Buesseler, S. C. Doney, S. F. Sailley, M. J. Behrenfeld, and P. W. Boyd (2014),
1226 Global assessment of ocean carbon export by combining satellite observations and food-web
1227 models, *Global Biogeochem. Cycles*, 28, 181–196, doi:10.1002/2013GB004743.
- 1228 Soetaert, K., P.M.J. Herman, J.J. Middelburg, C. Heip, C.L. Smith, P. Tett, and K. Wild-Allen
1229 (2001), Numerical modelling of the shelf break ecosystem: Reproducing benthic and pelagic
1230 measurements, *Deep-Sea Res. II*, 48(14-15), 3141–3177, doi:10.1016/S0967-
1231 0645(01)00035-2
- 1232 Somot S, Sevault F, Déqué M (2006) Transient climate change scenario simulation of the
1233 Mediterranean Sea for the twenty-first century using a high-resolution ocean circulation
1234 model. *Clim Dyn* 27(7–8):851–879.
- 1235 Somot, S., Houpert, L., Sevault, F. et al. (2016), Characterizing, modelling and understanding the
1236 climate variability of the deep water formation in the North-Western Mediterranean Sea.
1237 *Clim Dyn*, doi:10.1007/s00382-016-3295-0
- 1238 Stabholz M., X. Durrieu de Madron, A. Khripounoff, M. Canals, I. Taupier-Letage, P. Testor, S.
1239 Heussner, P. Kerhervé, L. Houpert, and N. Delsaut (2013), Impact of open-sea convection
1240 on particulate fluxes and sediment dynamics in the deep basin of the Gulf of Lions.
1241 *Biogeosciences*, 10, 1097-1116.
- 1242 Sverdrup H.U. (1953), On conditions for the vernal blooming of phytoplankton. *ICES J Mar Sci*
1243 (1953) 18 (3): 287-295. DOI:10.1093/icesjms/18.3.287.
- 1244 Taylor J. R. and R. Ferrari (2011), Shutdown of turbulent convection as a new criterion for the
1245 onset of spring phytoplankton blooms, *Limnology and Oceanography*, 56, doi:
1246 10.4319/lo.2011.56.6.2293.

- 1247 Uitz, J., D. Stramski, B. Gentili, F. D’Ortenzio, and H. Claustre (2012), Estimates of phytoplankton
1248 class-specific and total primary production in the Mediterranean Sea from satellite ocean
1249 color observations, *Global Biogeochem. Cycles*, 26, GB2024, doi:[10.1029/2011GB004055](https://doi.org/10.1029/2011GB004055).
- 1250 Ulses, C., P.-A. Auger, K. Soetaert, P. Marsaleix, F. Diaz, L. Coppola, M.Herrmann, F. Kessouri,
1251 and C. Estournel (2016), Budget of organic carbon in the North-Western Mediterranean
1252 Open Sea over the period 2004-2008 using 3D coupled physical biogeochemical modeling,
1253 *J. Geophys. Res. Oceans*, 121, 7026–7055, doi:[10.1002/2016JC011818](https://doi.org/10.1002/2016JC011818).
- 1254 Waldman R., S. Somot, M. Herrmann, P. Testor, C. Estournel, F. Sevault, L. Prieur, L. Mortier, L.
1255 Coppola, V. Taillandier, P. Conan and D. Dausse (2016) Estimating dense water volume
1256 and its evolution for the year 2012-2013 in the North-western Mediterranean Sea: an
1257 Observing System Simulation Experiment approach, *J. Geophys. Res. Oceans*, 121, 6696–
1258 6716, doi:[10.1002/2016JC011694](https://doi.org/10.1002/2016JC011694).
- 1259 Westberry, T. K., P. J. I. B. Williams, and M. J. Behrenfeld (2012), Global net community
1260 production and the putative net heterotrophy of the oligotrophic oceans, *Global Biogeochem.*
1261 *Cycles*, 26, GB4019, doi:[10.1029/2011GB004094](https://doi.org/10.1029/2011GB004094).
- 1262 Williams, R.G. and · M. J. Follows (2003), Physical transport of nutrients and the maintenance of
1263 biological production. in Ocean Biogeochemistry. Part of the series Global Change — The
1264 IGBP Series (closed) pp 19-51. Springer Berlin Heidelberg. doi:[10.1007/978-3-642-55844-](https://doi.org/10.1007/978-3-642-55844-3_3)
1265 [3_3](https://doi.org/10.1007/978-3-642-55844-3_3)
- 1266 Zúñiga, D., A. Calafat, A. Sanchez-Vidal, M. Canals, B. Price, S. Heussner, and S. Miserocchi
1267 (2007), Particulate organic carbon budget in the open Algero-Balearic Basin (Western
1268 Mediterranean): Assessment from a one-year sediment trap experiment. *Deep-Sea Res. I*, 54

1269 (9),1530-1548.